Form # 24

EXPERIMENT TECHNOLOGY DEVELOPMENT AND APPLIED RESEARCH WITH SLOW MONOCHROMATIC POSITRON BEAMS

THE SYMBOL OF THE PROJECT **PROJECT PAS**

DLNP, JINR: E. V. Ahmanova, M. K. Eseev[1], V. I. Hilinov, P. Horodek[2], A. G. Kobets[3], I. N. Meshkov, O. S. Orlov, A. Yu. Rudakov, K. Siemek[2], A. A. Sidorin, L. V. Soboleva, T. A. Stepanova, S. L. Yakovenko

[1]Northern (Arctic) Federal University named after M.V. Lomonosov, Arkhangelsk, Federal State Budgetary Institutions of Science Federal Research Center of Complex Study of the Arctic named after N. P. Laverov of the Russian Academy of Sciences, Arkhangelsk.

[2]Institute of Nuclear Physics Polish Academy of Sciences, Krakow, Poland

[3]Institute of Electrophysics and Radiation Technologies NAS of Ukraine, Kharkov, Ukraine

VBLHEP, JINR: V. M. Drobin, V. V. Seleznev

ITEP SIC "Kurchatov Institute": E. P. Prokopiev

The INP BSU, Minsk, Belarus: A. Ya. Silenko

University of Wales Swansea (UK): M.Charlton

PROJECT SUPERVISORS A. G. Kobets, P. Horodek

SCIENTIFIC PROJECT SUPERVISOR I. N. Meshkov

THE DATE OF SUBMISSION OF DRAFT TO THE SOD

DATE OF LABOROTORY SC 13.04.2017

DATE OF SUBMISSION OF THE PHYSICAL JUSTIFICATION AT THE LABORATORY SEMINAR 11.01.2017

Form # 25

PROJECT APPROVALS SHEET

EXPERIMENT TECHNOLOGY DEVELOPMENT AND APPLIED RESEARCH WITH SLOW MONOCHROMATIC POSITRON BEAMS

THE SYMBOL OF THE PROJECT **PROJECT PAS**

PROJECT SUPERVISORS A. G. Kobets, P. Horodek

SCIENTIFIC PROJECT SUPERVISOR I. N. Meshkov

APPROVED BY THE JINR DIRECTOR	_____ (Signature)	«___»_____ (Date)	**20 y.**
AGREED:			
JINR VICE-DIRECTOR	_____	«___»_____	**20 y.**
MAJOR SCIENTIFIC SECRETARY	_____	«___»_____	**20 y.**
MAJOR JINR ENGINEER	_____	«___»_____	**20 y.**
HEAD SOD	_____	«___»_____	**20 y.**
LABORATORY DIRECTOR	_____	«___»_____	**20 y.**
MAJOR LABORATORY ENGINEER	_____	«___»_____	**20 y.**
PROJECT SUPERVISORS	_____	«___»_____	**20 y.**
	_____	«___»_____	**20 y.**
SCIENTIFIC PROJECT SUPERVISOR	_____	«___»_____	**20 y.**
APPROVED PAC OF SPHERE	_____	«___»_____	**20 y.**

Content

Introduction 4
Studied problems and research objectives 4
The Low Energy Particle Toroidal Accumulator facility – creation and status 4
2. Low energy positron injector 11
2.1 The Cryogenic Source of Slow Monochromatic Positrons (CSSMP) 11
2.2 Structure of low energy monochromatic positrons injector 20
2.3. Positron Trap 22
3. Positron Annihilation Spectroscopy 29
3.1 Three PAS methods 29
3.2. DBAL spectrometer 31
4. The development of experiment technique 33
4.1. CSSMP 33
4.2. Creation of PALS spectrometer 34
4.3. Slow monochromatic positron specialized channel 35
4.4. The ordering flux of positrons 36
5. Expected outcomes upon completion of the project 39
Conclusion 40
Literature 40

Introduction

Studied problems and research objectives

The method of positron annihilation spectroscopy (PAS) is sensitive to point defects in a solid material. A pair of gamma quanta born by the process of positron-electron annihilation carries information about the concentration of defects with dimensions less than 10 nm at depths from the surface of the material, depending on the energy of the positrons (see section 3).

The installation PAS on the slow positron injector has two unique features:

- High monochromaticity of a positron flux – spectral width (FWHM) at the exit of the positron source is 1.5 – 2 eV;

- Positron Energy can be varied in the range of 1 – 35 Kev with an accuracy of not less than 1% on target.

The construction of the slow positron injector was completed in mid-2011, and the group have focused on experiments on the development of the method PAS. These works are scheduled to continue over the next three years, with the goal of creating a monochromatic positron special channel and experimental stations PAS, equipped with instrumentation for spectroscopy by measuring the lifetime of positrons in matter.

The Low Energy Particle Toroidal Accumulator facility – creation and status

The main goal of the LEPTA facility (Low Energy Particle Toroidal Accumulator) (Fig. 1) in the first years of its implementation (1999 – 2005) was the creation in JINR facility for generation of highly directional and monochromatic fluxes of positrons and positronium atoms in order to conduct fundamental experimental studies on such fluxes [I. 1, I. 2, I. 3]. Program of possible experiments, developed at that time, is of considerable interest today. At the same time the possibility of using the injector of slow monochromatic positrons created in the complex, for research in physics of solids using the method of PAS was understood. Such studies were initiated in 2013.

The experimental complex consists of the injector, storage ring and experimental channel (Fig. 1).

The design of the complex was started in December 1998.

In March 1999, began production of the first elements of a ring, in 2004, completed the construction and installation of a storage ring and in the ring 10.09.2004 obtained circulating electron beam from the test gun.

In 2006, a stand for test of the cryogenic source of slow monochromatic positrons was constructed (CSSMP) and it was conducted on a test emitter of low activity (made in DLNP JINR), resulting in a narrow range ($\Delta\varepsilon \sim 1.5$ eV) positrons, confirmed the efficiency of the design source. In 2008, was bought the emitter of positrons based on the ^{22}Na isotope (manufacture iThemba LABS, South Africa), activity of 25 MCI. In 2009, the cryogenic source (CSSMP) was assembled and tested at the stand with the emitter of iThemba; the resulting flux of slow positrons is of $1.2 \cdot 10^5$ s^{-1} with an average energy of 5.5 eV in the spectrum width (FWHM) of 2.3 eV.

2010 — completed the construction of the channel for transporting positrons from the source into the trap and started experiments on the accumulation of positrons and electrons (from test electron gun) in the trap and their rapid extraction.

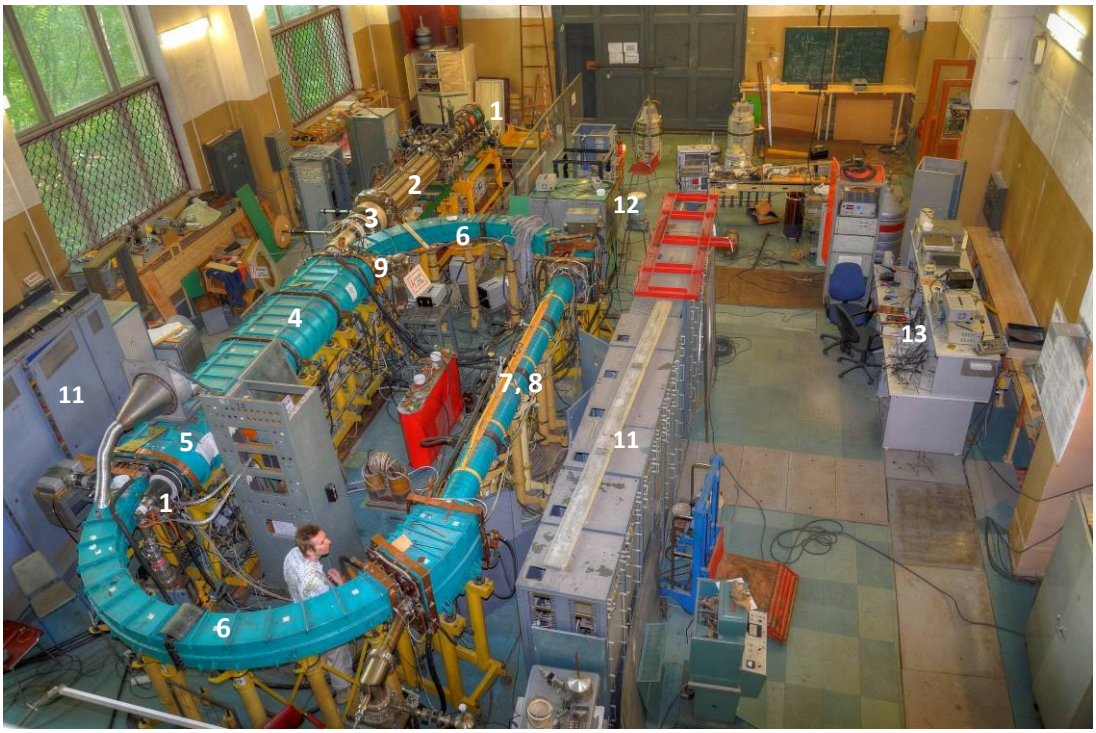

Fig. 1. General view of the complex: 1 — positron source, 2 — positron trap, 3 — positron injection channel, 4 — septum solenoids, 5 — kicker (inside septum solenoid), 6 — toroidal solenoids, 7 — solenoid and quadrupole coil, 8 — electron cooling section, straight solenoid, 9 — electron gun, 10 — electron collector, 11 — power supplies; 12 — experimental channel, 13 — remote control.

In 2010-2011 because of improving the focusing and the vacuum system of the ring, achieved the lifetime of electrons in the ring of 0.17 s. In 2011 was made a transport channel for the particles from the trap in the ring, obtained (September), a beam of positrons in the ring at the output of the kicker, and in 2012 held the positron first turn over ring, injected from the trap.

2012 — prepared a draft of the PAS spectrometer, which was commissioned in 2013 and the first PAS session was performed on the injector of slow positrons.

In experiments, 2012-2015 for optimizing the accumulation of particles in the trap has been found the explanation of the mechanism of compression of the beam in the trap under the action of the rotating electric field (the 2nd prize of JINR for the 2015 in experimental physics).

In 2014-2015, conducted 19 PAS sessions.

2015 — designed a new version of CSSMP with a closed cooling cycle based on helium cryocooler (section 4). In 2016, assembled a slow positron specialized channel (SPSC) and commissioned a new version CSSMP.

63 works published in 1995-2015 dedicated to the LEPTA project, including 11 in 2012-2015.

1. PAS applications (Добавить ссылки на работы)

There are three main classes of materials, which have so far been studied by means of PAS. Historically earliest PAS applications were devoted to studies of metals and alloys. Then PAS investigations were extended towards semiconductors. In both these fields positron plays a role of the main probe and formation of positronium (Ps) is usually of less significance. The third area of PAS applications, which is nowadays intensively being developed both in the experimental as well as theoretical planes, is concerned with studies of polymers and the other macromolecular substances containing large fraction of unoccupied space. Contrary to the above two kinds of materials, Ps is often formed with a high yield and becomes a principal probe in these systems. Below the some applications of PAS to materials` studies are shown.

1.1 Metals and alloys

Embrittlement in reactor pressure vessel steels

The nuclear reactor pressure vessel (RPV) is a key component if considering the safety of the nuclear power plant operation and possible lifetime prolongation. It is necessary to ensure the integrity of the reactor pressure vessel during normal and abnormal operating conditions. The ability of RPV to resist brittle fracture is of significant importance, especially under the loss of coolant accident conditions. The degradation of RPV steel is a complicated process depending on many factors (thermal and radiation treatment, chemical composition, manufacturing conditions, ageing, microstructure of the RPV material, operational history, etc.). These topics were studied in many comprehensive works.

Undoubtedly, the neutron embrittlement of RPV steels was a serious problem in Russian types of nuclear reactors (WWER-440, first generation V-230). It was caused mostly due to the narrower gap between the outside surface of the core barrel and the inside surface of the RPV as compared to Western RPV's. The relatively small diameter (Φin = 3542 mm in the case of WWER-440/V-230 type) facilitated transport and installation of the RPV, but, on the other hand, the neutron fluxes and consequently neutron fluencies on the RPV wall were generally several times higher than in other equivalent types in western Europe. This influence of neutron flux (even neutrons of energy over 0.5 MeV) on RPV embrittlement is much more impressive than contributions from a coolant temperature or an operational pressure in the primary circuit.

According to previous works it seems to be generally accepted that (even in those Western types of RPV steels containing more than 0.1 wt. % of Cu) Cu-rich and, depending on P content, P-rich precipitates play a dominant role in radiation induced embrittlement. In the case of WWER-type RPV steels, several studies have suggested that carbide formation is an important additional microstructural mechanism.

Due to long-term ageing and external loads including irradiation, the development of the fine scale defects occurs, which impede dislocation motion under applied stress. This process is the driving force for irradiation embrittlement. It leads to mechanical properties degradation, which can result, into the partial loss of plasticity and increase of the probability of brittle fracture. Defects are formed from vacancies and interstitials created in collision cascaded processes. Those point defects surviving the cascades migrate freely through the crystal lattice; interact with each other and with solute atoms in the matrix and also with dislocation substructure and precipitates. These irradiation-induced diffusion processes result into the formation of point defect clusters; dislocation loops and precipitates. Under the influence of temperature, the initial state of damage changes as a result of thermally activated migration of point defects, which is accompanied by their mutual recombination, annihilation on sinks and formation or dissociation of pile-ups.

These changes in the microstructure can be basically studied using several methods. Material properties of the steels and influence of thermal and neutron treatment on these properties are routinely investigated by macroscopic methods such as Charpy V-notch and tensile tests. A number of semi-empirical laws, based on macroscopic data, have been established, but, unfortunately, these laws are not completely consistent with all measured data and do not provide the desired accuracy. Therefore, many additional test methods such as positron annihilation spectroscopy (PAS) are used in this case [1.1].

Fatigue in aircraft wing

During service, aircraft wing panels have to endure a wide spectrum of mechanical and thermal loads. With the increase in average aircraft lifespan there is a clear need to increase our understanding of the fine details of fatigue damage. Aluminum aircraft alloys, such as AA2024, derive their excellent mechanical properties from the presence of nano-sized precipitates of well-tailored composition and dimension. It is the interaction of dislocations with these precipitates that is responsible for the high yield and tensile strengths values. The precipitate-dislocation interaction is also a key metallurgical parameter for the fatigue strength. While the development of dislocation networks in aluminum alloys during cyclic loading and the successive growth into microcracks (the accumulation of fatigue damage) has attracted a lot of attention in the literature, no studies have been performed on the fatigue damage of the actual precipitates themselves because of the enormous experimental challenges.

Based on existing dislocation-precipitate theories, it can be postulated that at least two potential precipitate fatigue mechanisms can occur: precipitate dissolution and loss of interfacial coherency. Precipitate dissolution is a real option for small precipitates because of successive precipitate shearing. The mechanism will lead to an increase in solute concentration and a very local loss of dislocation pinning force and a loss of strength at nanometer scale level. Alternatively, a repeated interaction of dislocations with larger sized precipitates may lead to an atomic restructuring of the semi-coherent precipitate-matrix interface. There are two options: the interface dislocation interaction increases the free volume at the interface via a deformation process or the amount of free volume decreases at the interface due to time dependent and possibly stress accelerated recovery. As with precipitate dissolution, the mechanism will lead to a reduction of precipitate pinning force and a reduction of local static and fatigue strength.

As the fatigue damage in precipitates occurs at the nanometer and sub-nanometer length scale, it will be clear that its experimental determination is extremely difficult. Even the most common technique for revealing the fine detail of precipitate and their interface structure, high resolution Transmission Electron Microscopy, is not very suitable, as the minimal amount of material probed does not easily provide representative information. It is only due to the recent advent of new physical characterization techniques. Such information can be obtained by PAS. Preliminary measurements on a 30 year old aircraft wing section made out of AA2024-T3 alloy revealed shifts in the positron annihilation curves suggesting a change in the free volume at the precipitate matrix interface. [1.2]

Corrosion

Corrosion is the destructive attack of a metal by chemical or electrochemical reactions with environment, which causes creation of oxides in material as well as worsens of material coherence. Therefore, atom binding can be broken and due to this and due to diffusion processes material lattice tries to relax. During the process of relaxation, some new structural defects can be formed. Degradation effect on lattice and its defect presence has already been investigated by Zhang et al. who demonstrated a growth of positron mean lifetime with an increase of chlorine content in environment for duplex (Cr-Ni) austenitic steel. This paper also indicated an increase of defect size and a slightly decease of defect concentration with

the increase of chlorine presence in the environment. Further, Pietrzak et al. studied low-alloyed steels in vapour of hydrochloric acid at 140 ^{o}C. These steels were exposed for 100 hours in this atmosphere and then their vacancy defects were larger and the concentration increased. These experiments can lead to assumption that positron annihilation spectroscopy is useful tool in corrosion degradation studies. Steels applied in nuclear facilities have to have very good resistance to corrosion, thus the investigation of the material degradation due to corrosion can be very useful even in condition of microstructural changes [1.3].

Ultra fine-grained metals

Over the past several decades, it has become known that the refinement of grain size of the traditional polycrystalline metals below one micrometer can lead to a significant improvement of their mechanical, electrical, thermal, and other properties. This is why ultra-fine-grained (UFG) metals, which are characterized with a mean grain size of several hundreds of nanometers, are nowadays attracting much attention of materials researchers as promising materials for various industrial applications. Among the methods of production of the UFG metals, those based on severe plastic deformation (SPD) are of a great importance. Macroscopic amounts of UFG materials with no porosity can be obtained by means of SPD. The following important elements of the SPD-created UFG structures can be outlined:

(i) Grains of the size of several hundreds of nanometers, which becomes comparable to typical diffusion lengths of free positrons in metals (≈ 100 nm).

(ii) Grain boundaries (GB) whose integrated volume constitutes, contrary to the ordinary polycrystalline metals, a significant fraction of the total volume of the material.

(iii) Defects introduced by SPD (dislocations, vacancies and vacancy clusters, GBs).

The two techniques utilizing SPD have recently been introduced to produce UFG structures in a wide class of metallic systems:

(a) The high-pressure torsion (HPT) is a technique capable to provide disk- -shaped specimens of the diameter of ≈ 10 mm and thickness of 0.2÷0.5 mm. The HPT-made specimens exhibit rather small grain size of ≈ 100 nm, homogeneous UFG structure, and a weak texture only.

(b) The equal channel angular pressing (ECAP) can produce more massive specimens, however, the mean grain size usually appears to be larger compared to HPT.

SPD process results in a highly non-equilibrium structure. It seems obvious that defects play a key role in formation of the UFG structure and lie beneath the extraordinary properties of these materials. Detailed defect investigations become thus highly desirable from the point of understanding the formation and thermal stability of the UFG structures. PAS thus seems to be an ideal tool for the investigation of the above listed UFG structure elements [1.4].

1.2 Semiconductors.

Atomic defects in semiconductors are electrically active and play a significant role in the electrical and optical properties of the materials. The defects induce localized electron levels, which act as trapping, recombination and scattering centers for free carriers. The localized levels can be detected by various spectroscopies. However, the identification of the atomic structure of the defects has turned out to be difficult. Positron annihilation as a defect-spectroscopic technique has three advantages. First, it has a specific sensitivity to vacancy-type defects which makes their identification straightforward. Second, the positron spectroscopy is strongly supported by theory, as the experimental signal from electron-positron annihilation can be theoretically calculated. Third, positron annihilation can be applied to any material independent of its doping and conductivity.

$CuInSe_2$ - solar cell thin films

Chalcopyrite semiconductors are suitable materials for optoelectronic devices due to their direct band gaps. So far, they have been mainly used as absorber materials in polycrystalline thin film solar cells. The thickness of the required layer is often below 2 μm, contributing to the potential for this technology to produce cheap photovoltaic devices. $CuInSe_2$ (CIS) and its derivative $Cu(In,Ga)Se_2$ have been used as absorber for high efficiency photovoltaic devices which result in stable device performance. The conversion efficiency of laboratory thin film CIS-based solar cells has surpassed 20%. $CuInSe_2$ has a direct band gap of about 1.05 eV that is close to the optimum band gap for solar cell of $E_{g,opt}$=1.35 eV, as it was calculated by Henry for terrestrial conditions. Compared to the other known semiconductors, CIS has the highest absorption coefficient; it exceeds 105 cm^{-1}. The electric properties of polycrystalline CIS thin film solar cell are strongly influenced by the presence of defects. These defects include native point defects (vacancies, divacancies, interstitials, etc.) and extended defects (dislocations, grain boundaries, etc.) that result from deviations from the stoichiometric composition caused by the preparation process. The defect physics of CIS is known to be complicated due to the great number of native defects and complex defects. However, understanding of the performance of CIS requires knowledge about defects, which are expected to dominate its properties. This knowledge can be provided through the PAS methods [1.5].

ZnO – optoelctronic applications

Over the years, the polycrystalline zinc oxide (ZnO) has been found to have wide applications including piezoelectric transducers, varistors, phosphors, and transparent conducting films. As a wide-gap (3.37 eV at room temperature) semiconductor, it is now attracting more attention. Recent success in producing large-area single crystals revealed that ZnO has potential optoelectronic applications in blue and UV light emitting devices due to the wide band gap and large exciton binding energy (60 meV). The close match in the lattice constant with GaN also allows it to be a good substrate material for GaN based devices. ZnO is well poised for space applications, since it is fairly resistant to radiation damage compared with other semiconductors.

The key factor to assure the high performance of semiconductor devices is high quality crystals. However, in semiconductors various defects often exist which affect the electrical and optical properties. In ZnO, for example, undoped materials mostly exhibit *n*-type conductivity. This is supposed to be due to the existence of native point defects, such as oxygen vacancies and Zn interstitials. Like many other wide-gap semiconductors, there exists a so-called doping asymmetry, that is, it is easy to get *n*-type ZnO, but rather difficult to produce *p*-type ZnO. One of the possible mechanisms leading to the doping difficulty is the selfcompensation by native defects, which has prevented the production of ZnO based devices such as UV-emitting diodes. Some defects also reduce the device lifetime and decrease the light emission efficiency. For example, dislocations act as nonradiative recombination centers and suppress the UV emission. Control of the defects to improve the quality of the materials has been proven to be very important. Study of the microstructure of these defects in ZnO is necessary to provide the guidance to control these defects [1.6].

TiO_2 photocatalyst

Since the discovery of water photolysis on a TiO_2 photoanode by Fujishima and Honda in 1972, semiconductor photocatalysis has attracted significant attention due to its promising application in environment remediation and solar energy conversion. Semiconductor materials are the most important issue in heterogeneous photocatalysis research and a variety of materials has been developed as possible photocatalysts so far. Among all the semiconductor materials investigated, TiO_2 is regarded as a benchmark photocatalyst under ultraviolet irradiation because of its superior photocatalytic activity, good chemical stability

and high resistance to photocorrosion. Extensive research has been carried out on the application of TiO_2 as a photocatalyst in various reactions and distinctly different photocatalytic properties have been reported. It is generally acknowledged that the photocatalytic performance of TiO_2 samples can be greatly influenced by their physico-chemical properties, especially crystalline phases, exposed crystal facets and surface/bulk defects. PAS studies shows the effects of surface/bulk defects should not be ignored when discussing the photocatalytic activity of TiO_2 or other semiconductor photocatalysis systems [1.7].

1.3 Polymers and porous materials

Nanoporous materials have a diverse array of industrial applications that largely stem from their extremely high surface areas, which provides sites that can be functionalized (for instance, in catalysis), and their free volume, enabling the capture and separation of molecules. Nanoporous solids are thus extensively employed as (for example) adsorbents, catalysts, gas sensors, bio-membranes and polymeric selective permeation filters. As the functionality of nanoporous materials is specified by their pore characteristics (including size and concentration), the pore structure of such solids is tailored for particular applications, and numerous techniques, such as molecular adsorption (using N2, CO2 and other probe molecules) and mercury porosimetry, have been developed as characterization means. However, most of these approaches come with limitations as they rely on the solid having interconnected pores large enough to allow the passage of a probe atom or molecule through the material. Imaging techniques like TEM (transmission electron microscopy) are capable of revealing nano-scale pore information, but they too require extensive sample preparation, which can alter the pore distribution. The characterization techniques available to the growing field of nanoengineering thus require dramatic improvement, as few methods like PAS are able to characterize nano-scale porosity, particularly when the pores are closed and consequently inaccessible to gas adsorption methods. Positron annihilation lifetime spectroscopy is an important method for studying such subnanometer size holes and for the determination of their size distribution and free-volume fractions. In a polymer or porous matrix, thermalized positrons can form positronium (Ps) that will be localized in free-volume holes. The primary annihilation mechanism of the long-lived triplet state of positronium (ortho-positronium, o-Ps) is the pick-off annihilation with electrons of the host medium, with annihilation parameters dependent on the physicochemical properties. The lifetime and intensity of this component can be translated into hole size and density.

Polyurethanes Membran

Polyurethanes, extensively used in the chemical industry, usually consist of hard segments (urethane/ urea groups and/or low molecular weight chain extenders) and one or more soft segments (e.g., polyether/ polyesters). Depending on the processing parameters and on the type of hard and soft segments these can be totally mixed or phase-separated to different degrees. This structure versatility enables the production of materials with a wide range of properties. One important application of urethane/urea membranes is the exploitation of their selective permeability in industrial separations, namely gas permeation and pervaporation. The free-volume concept is extensively adopted in polymer science to explain many properties at microscopic structural level and to relate them with macroscopic properties. PAS studies allows characterizing nano-scale porosity for these membranes [1.8].

Adsorbtion

Volatile organic compounds (VOCs) are emitted to the atmosphere from different sources. Their emissions accompany not only many manufacturing processes in the chemical, petrochemical and pharmaceutical industries etc., but VOCs are also released from commonly used products such as paints, paint thinners, varnishes, solvents, hydraulic fluids, cosmetics, and dry-cleaning agents. However, the emission of gasoline vapor during its

production, storage, transportation, and use can be considered the largest emission source of VOCs. Gasoline consists of hydrocarbons with chains containing 4–12 carbons (C4–C12), and mostly consists of paraffin's (alkanes), cycloalkanes (naphthenic), and olefins (alkenes). The vapor of gasoline is mostly a mixture of light hydrocarbons (C4–C7s), which are significant components of VOCs. The recovery and reuse of evaporated gasoline are of vital importance from both economic and environmental points of view. Additionally, the highly efficient recovery of marketable VOCs might significantly offset the cost of emission control. Therefore, many efforts have been made to find appropriate technologies for separating and recovering VOCs from polluted air streams. Adsorption is one of the most commonly used and practical methods for the separation and recovery of VOCs, as well as for controlling VOC emissions. Thus, a very important issue for VOC adsorption processes is to employ suitable adsorbents that exhibit appropriate chemical properties, a high specific surface area, a high regeneration ability, and physical stability. Activated carbons have been considered as one of the most attractive adsorbents given their excellent adsorption capacity. However, all adsorbents have certain advantages as well as limitations. Therefore, other adsorbents such as hydrophobic silica gels, delaminated Y zeolite, and hypercrosslinked polymeric adsorbents have also been extensively investigated to separate and recover gasoline vapors. Over the past few years, positron annihilation lifetime spectroscopy (PALS) has been shown to be a powerful technique for obtaining information concerning the mechanism of adsorption and desorption of gases.

Zeolites

Zeolites are commercially available and extensively used as 'molecular sieves' adsorbing gases and liquids in, for example, catalysis and radioactive waste management, oil cracking and animal feed supplementation. Zeolites are aluminosilicates with three-dimensional structures composed of separate SiO_4 and AlO_4 tetrahedral joined by shared oxygen atoms. In these structures are channels and cavities inside which cations and water molecules may be located – these channels and cavities in molecular sieves permit the adsorption of molecules smaller than the pore dimensions, whilst rejecting others based on their larger molecular dimensions. In fact synthetic zeolites known as 'Molecular Sieve 3Å, 4Å and 5Å' are common in research labs, especially chemistry labs, where they are used to dry gas lines. The research group also uses zeolites in foreline pumps to adsorb oil vapour. PAS methods in this case are used for characterization of sizes and pores distributions, which are responsible for properties of zeolites [1.9].

2. Low energy positron injector

The injector for PAS method should provide not less than $1 \cdot 10^8$ slow monochromatic positrons per second. The choice of positron emitter, its settings and design are largely determined the injector structure described below.

2.1 The Cryogenic Source of Slow Monochromatic Positrons (CSSMP)

There are several schemes to produce intense positron beams. Positrons can be generated by using synchrotron radiation, where the photons interacting with the target are converted into electron-positron pairs. In scheme with linear electron accelerator beams of positrons formed in the conversion of the electron beam on the target ($e^- \rightarrow \gamma \rightarrow e^- e^+$). In the scheme with β^+ emitter a positron source is the radioactive isotope. In any of the above schemes, the positrons have a broad energy spectrum. Positrons slows in solid target for the formatting slow monochromatic beams from such spectrum.

In the scheme with a linear accelerator, the maximum obtained number of slow positrons is of 10^{10} e^+/s [2.1]. In the scheme with the source of synchrotron radiation is expected to

receive up to 10^{12} e^+/s [2.2]. For the scheme with a radioactive isotope, the intensity of slow positrons does not exceed 10^7 e^+/s. However, the first two schemes are cumbersome; require large capital expenditure and radiation protection. At the same time, the scheme with a radioactive isotope is small, cheap and radiation protection is relatively simple.

In the scheme with linear accelerator [2.3] as a moderator one uses a set of tungsten plates, from which slow positrons are extracted by a combination of electric and magnetic fields. In this scheme, the maximum yield of positrons is limited to thermal and radiation loads that can sustain the target in contact with the electron beam. Table 1 lists the centers for obtaining slow positrons based on linear accelerator parameters of facilities.

Table 1. Research centers, producing slow positrons based on linear accelerator

Research center	Energy of electron beam, MeV	Electron beam current I, μA	Slow positrons yield e^+/s
Giessen (Germany)	65	100	10^8
Arhus (Denmark)	100	0,1	10^6
Livermoore (USA)	100	600	10^{10}
Oak Ridge (USA)	170	300	10^8
Rossendorf (Germany)	250 1000	100 100	$3\cdot10^9$ 10^{10}
KEK (Japan)	50		10^8

The generation of bright beams of slow positrons by using synchrotron radiation (SR) became possible with the development of powerful sources of SR is able to generate an intense photon flux with energies above 1 MeV. The attempt to create such a source on the drive SPring-8 (Japan) [2.4], with an electron energy of 8 GeV, which is a record according to the characteristics of SR. The source of slow positrons also consists of a target and moderator in the form of tungsten plates. As a powerful source, Spring-8 uses unique superconducting wiggler with a field of 8-10 Tesla, manufactured in BINP [2.5]. The work had to stop because of the unacceptably high level of SR. The uniqueness of this source of slow positrons was the fact that it was first supposed to carry out a direct conversion of the hard part of synchrotron radiation to the positrons. The expected intensity of this source was of about 10^{12} e^+/s.

The widespread use of β^+-active isotopes started in the 70-ies of the last century with the development of technology for the effective formation of a monochromatic flux of slow positrons from a wide β^+-spectrum of the isotope. The possibility of slowing down of positrons was first proposed by Madansky and Rasetti in 1950 [2.6], but the first successful result was obtained by Cherry in 1958 [2.7]. He observed positrons with energy less than 10 eV emitted from the ^{22}Na source using mica coated with a thin layer of chromium. The conversion efficiency ε of the spectrum — the ratio of the number of slow positrons from the moderator to the total number of fast before slowing, was very low, $\varepsilon = 3\cdot10^{-8}$. In 1972 Costello and others. [2.8] experimentally confirmed the possibility of thermalization of positrons in a solid, watching the emission of positrons with an energy peak between 0.75 - 2.90 eV from the moderator, covered with gold with a thickness of 0.02 microns. Mills and Pfeiffer [2.9] developed the first effective moderator in 1979. As moderator was used crystal copper (111), placed together with a radioactive isotope into the chamber to ultrahigh vacuum. The effectiveness of moderation was $1\cdot10^{-3}$. Currently, the efficiency increased by almost on order, and now in modern sources, it reaches the level of $\varepsilon \sim 1\cdot10^{-2}$ [2.10].

The most effective and convenient of radionuclides used in research as sources of positrons (table 2) is the isotope ^{22}Na. The half-life of the isotope is 2.6 years making it suitable for long-term experiments. This isotope gives a relatively high yield of positrons ~ 90,5% in a wide energy spectrum (table 2). In addition, there was developed a well-established technology of its production, which ultimately affects the table cost of the isotope.

Table 2. The characteristics of positron-active radionuclides used in research

Isotope	Half-life period	Maximum positron energy, MeV	The ratio of decays, %
^{22}Na	2.603 *years*	0.545	90.50
^{44}Ti	47.3 *year*	1.467	98
^{48}V	15.974 *days*	0.696	50.7
^{55}Co	17.54 *hours*	1.50	60
^{56}Co	78.76 *days*	0.421	1.03
^{57}Ni	36 *hours*	0.85	50.0
^{58}Co	0.79 *days*	0.475	15.05
^{64}Cu	12.703 *hours*	0.652	17.9
^{65}Zn	243.9 *days*	0.329	1.45
^{68}Ge	288 *days*	1.899	87.52
^{90}Nb	14.6 *hours*	1.50	54

The reasons above led in to the choice of the emitter of positrons based on the ^{22}Na isotope. These emitters are manufactured at the laboratory iThemba LABS[*]) (Capetown, South Africa).

Created at JINR the Cryogenic Source of Slow Monochromatic Positrons (CSSMP) is a main element of the slow positron injector. High-energy positrons emitted in the decay of the isotope ^{22}Na, pass through in a solid moderator, where they lose their energy to ionization losses and (below ionization threshold) through the creation of a pair electron-hole excitons and phonons slow down to thermal speeds. As moderator is selected solid neon. This is because the positrons emitted by the ^{22}Na isotope have a wide energy spectrum with a maximum at energy of about 200 Kev (Fig. 2). For the formation from this spectrum a monochromatic beam of low energy positrons is used moderator, which is characterized by the deceleration efficiency ε and the width of the spectrum of slow positrons.

[*] Laboratory for Accelerator Based Science

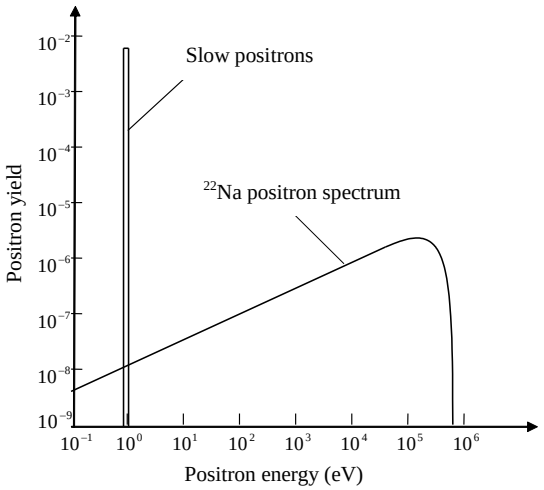

Fig. 2. The range of positrons emitted by ^{22}Na before and after passing frozen neon on the output of the emitter foil.

"Thermal" positrons can diffuse to the surface of the moderator, and leave the substance or "stuck" in matter and annihilate with one of the atomic electrons directly or with the formation of positronium (mainly in the para-state — p-Ps) (Fig. 3). The solid matter is characterized by "work function" the positron release from the surface φ_+ equal to the difference between the values of the potential energy of the particles inside the solid body (~ 1 Å from the surface) and at an infinite distance from it. The absolute value of the work function is about 1 electron volt, and $\varphi_+ > 0$_is a potential barrier formed at the transition surface-vacuum which prevents the release of thermal positrons. The most effective moderator is a solid neon (Table 3) — insulator with large band gap and a lack of free electrons. For this reason, the neon $\varphi_+ > 0$, which prevents the escape of thermal positrons. The presence of a wide forbidden zone leads to the fact that a positrons are not thermalized completely inside the material and therefore have a greater length of run. As a result, they have sufficient energy to overcome the potential barrier "matter-vacuum" and have a wider energy spectrum.

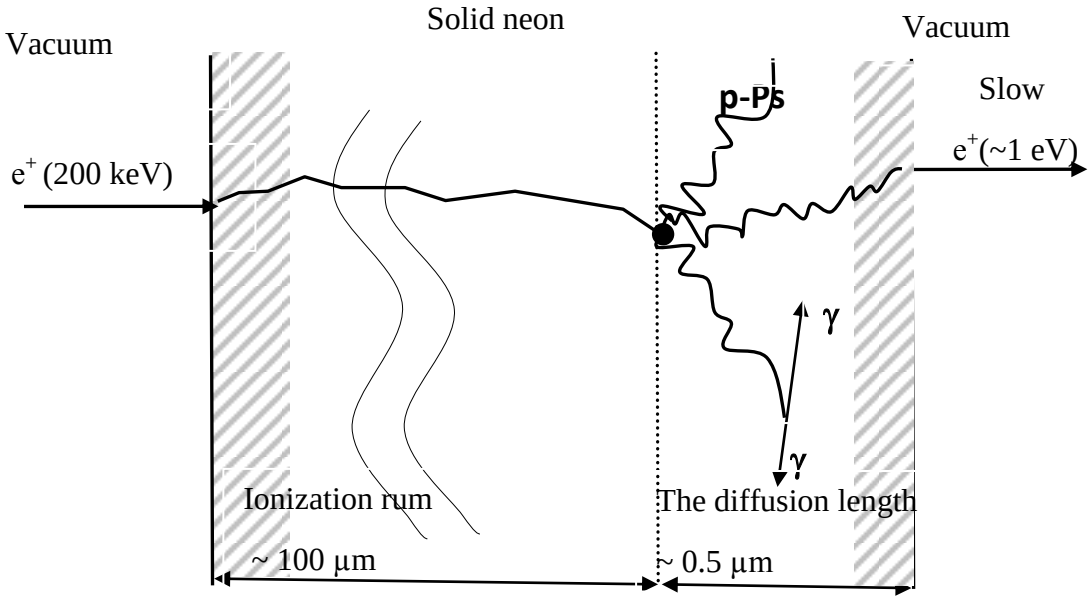

Fig. 3. The process of slowing down positrons in solid neon

Table 3. The efficiency of different moderating materials

Material	State	Efficiency
MgO	Polycrystalline powder	$3 \cdot 10^{-5}$
Cu(111)	Monocrystal	$1 \cdot 10^{-3}$
B	Carbon-coated polycrystal	$\approx 10^{-7}$
W(110)	Monocrystal	$3 \cdot 10^{-3}$
Ne	Solid neon at 5 K	$7 \cdot 10^{-3}$

To achieve the maximum yield of slow positrons from the moderator thickness of the layer of solid neon is necessary to select approximately equal to the ionization path length of the positron at an energy corresponding to the maximum of the spectrum of positrons emitted by ^{22}Na (Fig. 2). Caused by the slowdown in solid neon from a wide energy range of positrons emitted by ^{22}Na is formed a narrow spectrum of slow monochromatic positrons (Fig. 2)

Solid neon so is used usually in sources as a moderator. The process of "growing" moderator begins with cooling of the substrate emitter to a temperature of 5K, and then in a vacuum chamber, which encloses a radioactive isotope, a gas of neon is injected and partially condenses on the substrate forming a solid moderator. Such a scheme of the moderator formation has a number of disadvantages: neon condenses non uniformly on the surface of the substrate, there is no possibility to control the thickness of the moderator, and the process of freezing proceeds with change of vacuum conditions. The scheme of the moderator formation proposed at injector and design of CSSMP (Fig. 4, 5) allow eliminating these disadvantages: pre-cooled gaseous neon is formed as directed flow of cooled neon through nozzles directly onto the substrate. The advantage of this scheme is the possibility of controlling the thickness of the frozen layer by the neon flow (jet) rate.

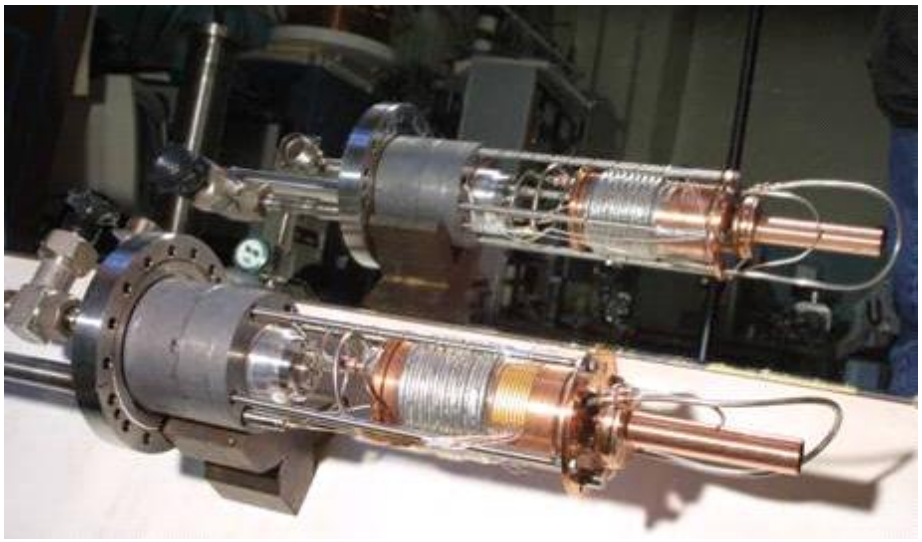

Fig. 4. The cryogenic Source of Slow Monochromatic Positrons (CSSMP)

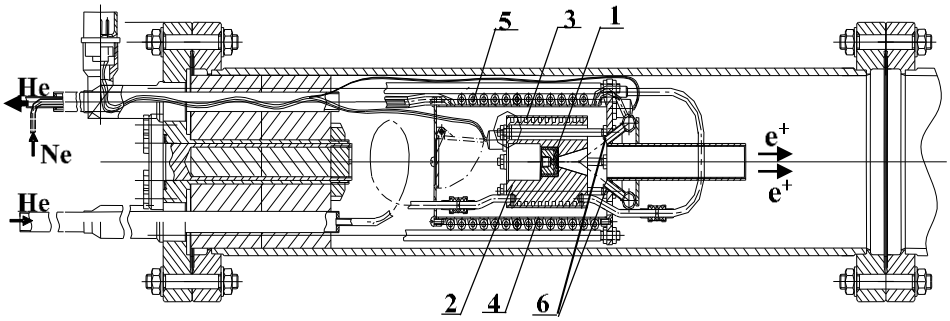

Fig. 5. The Cryogenic Source of Slow Monochromatic Positrons. 1 — copper substrate with the isotope ^{22}Na, 2 — copper cylinder, 3 — cryogenic heat exchanger that is a copper cylinder, 4 — heat shield, 5 — cryogenic heat exchanger of a heat shield, 6 — nozzle.

Source of CSSMP is located in a vacuum chamber (Fig. 4, 5). A tablet with a radioactive isotope ^{22}Na is placed on the copper substrate (1) which is placed inside the copper cylinder (2) in the cone-shaped hollow at the end of a cylinder. Similar design is described in [2.11]. Apex angle of cone is equal to 18°. These elements form a positron emitter block (Fig. 6), which is cooled to a temperature of a few Kelvin. On the surface of the cylinder is a cryogenic heat exchanger (3) through which flows cold gaseous helium at a temperature slightly above 4K that cools the emitter block. Copper cylinder (2) is placed inside a copper shell (4), which is a heat shield. On the outer surface of the shell is a second heat exchanger (5). Running through a heat exchanger (3), helium enters the heat exchanger (5) for cooling the heat shield. Gaseous neon enters the positron source through the heat exchanger shield (4), where it is pre-cooled and escapes to the surface of the cone-shaped hollow and on the end face of a copper substrate with an isotope through four nozzles (6). In the copper cylinder (2) and the shield (4) are located temperature sensors to control the temperature of the emitter block and a heat shield. The positron emitter block is electrically isolated from the heat shield. Positron beam energy can be controlled by applying to it the electrostatic potential in the range from 0 to 1 kV.

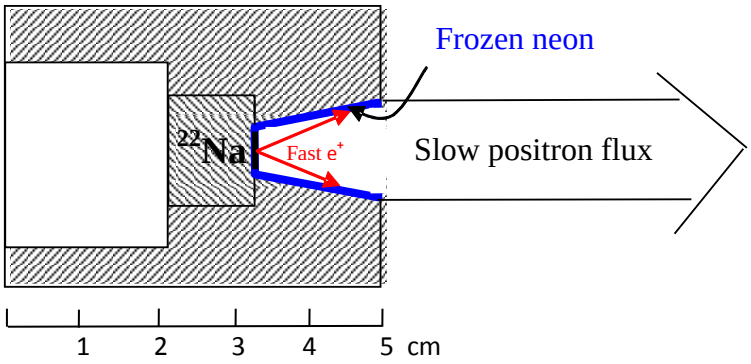

Fig. 6. Positron emitter block

The process of the freeze of the moderator begins after a stationary temperature is established in the cooled substrate. The main elements of the neon line (Fig. 7), which allow controlling the thickness of the layer of frozen neon, are a measuring volume and a choke with a large impedance Z.

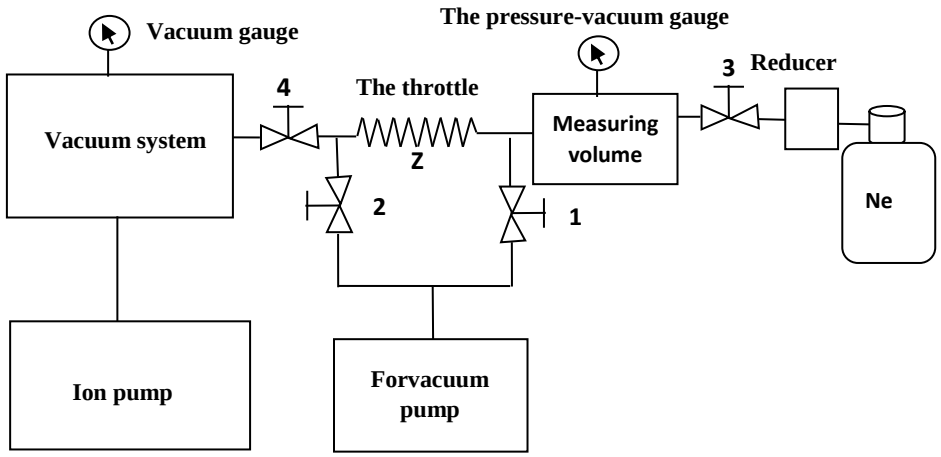

Fig. 7. A scheme of the line of overlap of the neon system. 1, 2, 3, 4 — vacuum valves

Before neon is injected in the system, injection line will be pre-pumping. The valves 3 and 4 are closed and through valves 2 and 1 measuring volume and the gas supply line between the throttle and the valve 4 are pumped. After preliminary pumping, valves 1 and 2 are closed. The valve 4 is opened in order to avoid a jump of the pressure in the system after the beginning of the gas injection. Chemically pure neon by the valve 3 is or from the container into the measuring volume up to a pressure of 0.5–0.7 at, and the valve 3 is blocked. From a measuring volume neon through the throttle and valve 4 flows into the system. The flow rate of the neon is controlled by the pressure-vacuum gauge.

The first experiments on measuring the characteristics of the source CSSMP were performed with a test radioactive isotope ^{22}Na of the activity of 0.8 MBq. "Positron Source" was equipped with devices for the separation of positrons and analysis of positron energy of the slow monochromatic positron beam (Fig. 8). CSSMP and microchannel plate (MCP) detector for registration of positrons were placed inside the vacuum chamber. Shutter was installed between them to prevent direct contact with positrons at the MCP. The vacuum chamber was placed into a longitudinal magnetic field. Before and after the shutter were situated coils of transverse magnetic field. They form a trajectory of slow positrons ("slalom"), rounding the shutter. MCP is located in front of the electrostatic analyzer — cylinder, which is set to analyze positron energy. In addition, outside of the vacuum chamber was installed the gamma-detector that detected positron annihilation gamma-quanta. Both detectors were calibrated with the reference β^+-active source. The methodology and results of calibration described in section 1.3.

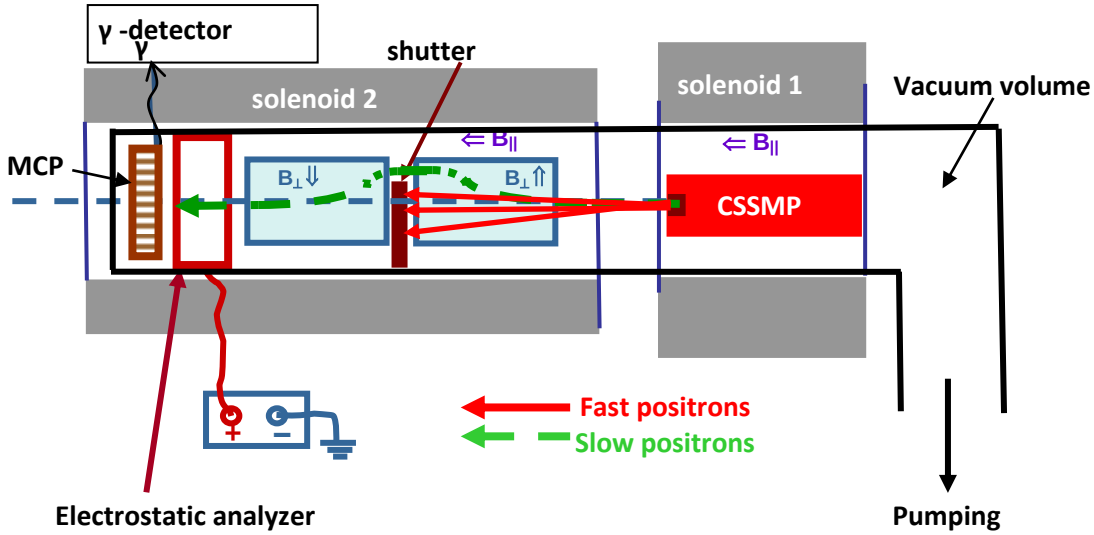

Fig. 8. Measuring scheme of the stand "Positron Source"

With increase of the thickness of the moderator occurs the growth of the yield of slow positrons (Fig. 9). The maximum yield of slow positrons corresponds to the moderator thickness of 130 microns. A further increase of the thickness of the moderator leads to a reduction, of slow positron flux.

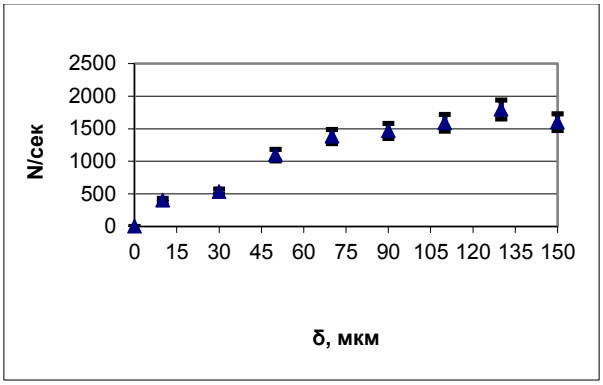

Fig. 9 The count of positrons vs the frozen moderator thickness (experimental points with statistical errors)

For the first time, the dependence of the shape of the spectrum of slow positrons on the thickness of the frozen layer was measured for this type of sources. The formation of the spectrum starts with the moderator thickness of 10 microns. With increasing thickness of frozen layer spectral density at the maximum increases (Fig. 10), and the width of the spectrum decreases (Fig. 11). The average energy of the emitted positrons decreases as well (Fig. 12).

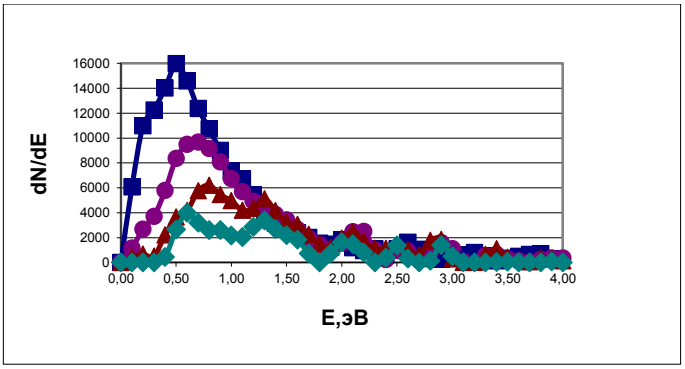

Fig. 10. The shape of the spectrum of positrons vs the thickness of the frozen moderator, μm: 30 (♦), 50 (▲), 90 (●), 130 (■).

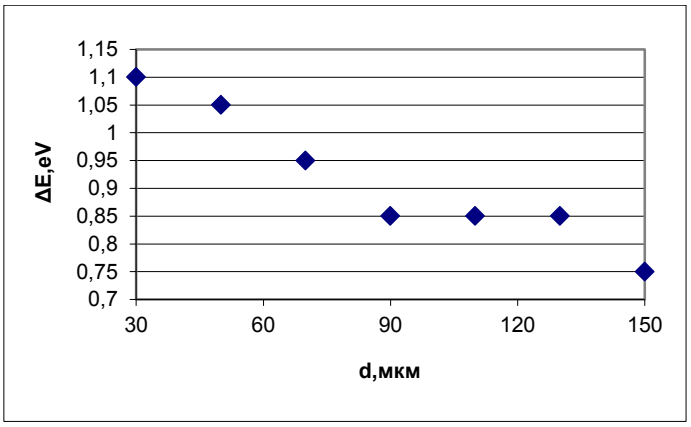

Fig. 11. The FWHM of the positrons spectrum vs the thickness of the frozen moderator

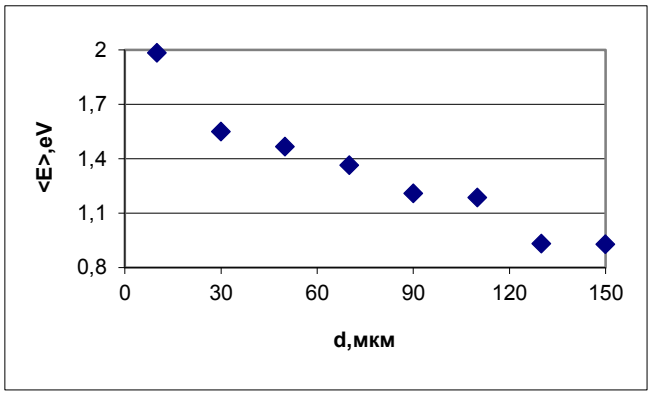

Fig. 12. The average energy of the slow positrons emitted from the moderator vs the thickness of the moderator

After the freezing end the yield of positrons continues to grow for several hours. The number of recorded slow positrons increases by 12% (Fig. 13).

After optimization of the moderator thickness and turning of the registration system the maximum count rate was reached. Taking into account the efficiency of the MCP (30%), the deceleration efficiency was ε = 1% and FWHM of the positron spectrum of 1 eV (Fig. 14). The average energy of positrons can be varied by application of a potential to the emitter.

Fig. 13. An example of the evolution of the slow positrons yield after the end of moderator freezing

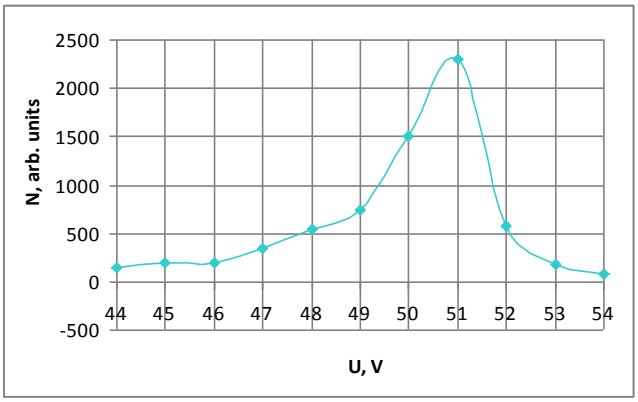

Fig. 14. The typical spectrum of slow positrons from the CSSMP

2.2 Structure of low energy monochromatic positrons injector

To provide the ability to inject short positron bunches, the positron injector is equipped with Penning–Malmberg–Surco trap (PMS).

The prototype of the positron trap was the trap used in the experiments for obtaining antihydrogen ATHENA (ALFA) CERN [2.12]. The number of stored positrons is about 10^8 particles [2.13].

The choice of a particular source type is determined by the capture efficiency of the trap and the desired repeated rate of pulses injected into the storage. When the pulse frequency of injection is 0.01 Hz and the efficiency of capture in the trap 30 % the required average flux of positrons entering the trap is $5 \cdot 10^6$ to 10^7 positrons per second. This flow rate can be obtained from radioactive isotope ^{22}Na activity 25÷50 MCI. A higher pulse frequency of injection is possible when using a source with greater average intensity, for example, based on linear electron accelerator.

In the result of the analysis the scheme based on a radioactive isotope was chosen and injector of positron was developed, corresponding to the number of positrons per pulse (Fig. 15). It is composed of:

- the source of positrons CSSMP (Fig. 15, POS. 1),
- transport channel of low energy positrons from the source to the trap,
- particle trap Penning–Malmberg–Surco type (POS. 2),
- a channel for transporting the particles with their acceleration up to energy of the experiment (Fig. 3).

The acceleration of particles is accomplished by a static electric field in the gap of the bushing insulator (Fig. 15, POS. 11) that separates the part of the injector, "suspended" under potential (1-10 kV), from part of the channel and a ring having zero potential. Accelerating gap electrode has a special shape (Fig. 16) providing the adiabatic acceleration of particles.

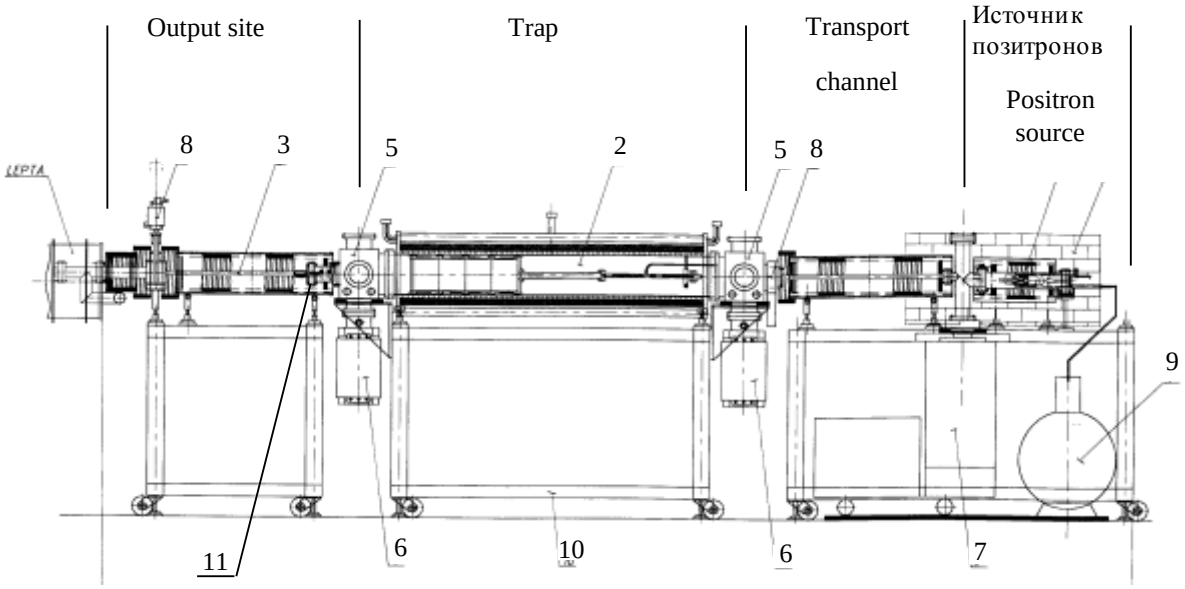

Fig. 15. Positron injector. 1 — positron source, 2 — positron trap, 3 — injection part of the positrons in the accumulator, 4 — radiation shield, 5 — vacuum post, 6 — ion pumps, 7 — turbo molecular pump, 8 — gate, 9 — Dewar vessel, 10 — prop, 11 — bushing isolator.

After moderator, monoenergetic positron flux with an energy of 50 eV enters the transport channel. The small diameter of the vacuum chamber of the transport channel prevents the penetration of neon from the source area to the trap, what increases the life time of positrons in it, depending on the composition of the residual gas. In addition, the transport channel is used for separation of positron by energy: the axis of the vacuum chambers of the positron source and transport channel are shifted relative to each other vertically, and a special superposition of a longitudinal field of the solenoid and an additional transverse magnetic field provides to ingress only slow positrons into the trap of. Positron trap is designed to accumulate positrons, which are held in it by the magnetic field of the solenoid and electric field of a system of electrodes arranged in a vacuum chamber. The accumulation process lasts about 10÷100 seconds, while the positrons are cooled to room temperature by collisions with the molecules of the "buffer gas" (nitrogen). With optimal allocation of buffer gas pressure and electrostatic potential along the trap its efficiency (the fraction of captured positrons) is 30 % [2.14]. Pumping all nodes of the injector is oil-free pumps, as positrons annihilate active on the molecules of hydrocarbons.

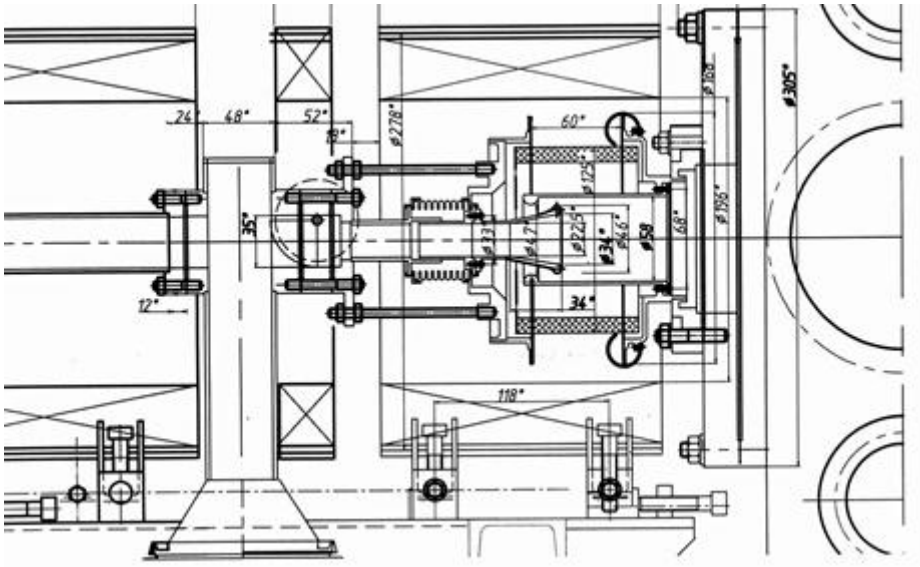

Fig. 16. The positron acceleration section

The injector, from the emitter to the entrance of the ring is located in a longitudinal magnetic field, which varies from 200 to 400 Gauss in the channels and is set to 1.2 kG in trap.

2.3. Positron Trap

Charged particle traps was proposed, created and used for the accumulation and prolonged retention of the particles for three purposes:

- carrying out of experimental measurements with maximum possible accuracy of the parameters of both the particles and various nuclear, atomic and molecular objects they formed,
- formation of a dense hot plasma of hydrogen isotopes in fusion generators,
- as auxiliary sections for various experimental systems for the accumulation, separation, cooling and compression of charged particle beams before their injection into other elements of the complexes for further experiments.

Such devices are widely used in atomic and nuclear physics, accelerator physics, mass spectrometry, plasma installations. Research in the field of exotic atom physics and antimatter initiated the development of technology accumulation, retention, and control bunches of charged particles (antiparticles). This can be done in electromagnetic open system with controlled injection of charged particles and clumps of accumulated particles. For the accumulation of charged particles, the most common is the Penning trap with a longitudinal magnetic field and quadrupole electrostatic potential and the Penning-Malmberg trap with cylindrical electrodes. For the accumulation of positrons from radioactive sources K. Surco proposed to use a buffer gas with a pressure distribution along the trap, consistent with the distribution of potentials on the cylindrical electrodes. This advanced Penning-Malmberg-Surco (PMS) trap has been successfully used in many laboratories of the world in experiments with ions, positrons and positronium:

University of California, San Diego and riverside positrons and Positronium;

CERN — ATHENA/ALPHA, ASACUSA, AEgIS — accumulation of positrons and antiprotons for antihydrogen generation and experiments;

complex ISOLDE — radioactive beams "factory";

Michigan State University, Argonne National Lab. (USA), GSI (Germany), GANIL (France), TRIUMF (Canada) — radioactive beams "factory".

At JINR such trap was created as part of the injector of slow positrons with a goal to their further accumulation and injection into a storage ring. The possibility of using such traps for the accumulation of radioactive nuclei at FLNR JINR and laboratory of iThemba LABS is considered (South Africa).

A significant step in the development "traps" technology was the use in traps of PMS rotating electric field perpendicular to the axis of the trap: increased efficiency of accumulation of the particles and their life time. Moreover, best of all, a bunch of accumulated particles in a longitudinal magnetic field is compressed in the presence of the rotating field — the effect of the so-called "rotating wall" ("Rotating Wall" RW). Found on positive ions [2.15], the effect of the RW-field has been successfully used for the accumulation the electron and positron plasma, to study the properties of antimatter and exotic atomic and molecular systems. In the literature so far has not been a clear mechanism for such action of the field.

PMS trap injector [2.16, 2.17] has the traditional PMS trap geometry (Fig. 17). In 2013-2014, trap pumping significantly improved [2.18]: installed turbomolecular and cryogenic pumps. The choice of the potential distribution of the electrodes 1-8 and the pressure of the buffer gas (high-purity molecular nitrogen) is critical. With the best possible distribution of pressure and potentials positrons, "crossing the line" at the atomic and molecular levels, very quickly passes the region of energy where the probability of annihilation of a maximum – the so-called "Ore Gap".

Rotating electric (RW) field is generated in the electrode 4, cut into 4 sectors that are served on constant and (pairwise) variable potentials. Typical amplitude RW-voltage on sector electrode is 1 V.

The positron emitted by the cryogenic source CSSMP (section 1.1) developed in JINR.

Positrons accumulated in the trap are thrown to the collector (Fig. 16, POS. 9), and scintillation counter are recorded born the annihilation gamma rays in analog mode. The sensitivity of the counter calibrated on the reference β^+source and is $N_{trap} = 6.66 \cdot 10^3 \cdot V_{[V]}$ positrons, $V_{[V]}$ — signal amplitude in volts. The signal from a single positron has an amplitude of V_1 = 10 mV. Hence, the statistical error of the measurement is $\Delta N_{\text{trap}}/N_{\text{trap}} = 0.1/\sqrt{V_{[V]}}$. A flux of positrons injected into the trap, measured with the same counter in the counting mode when trap opened $N_{e^+} = 66.6 * \dot{N}_{counts}$.

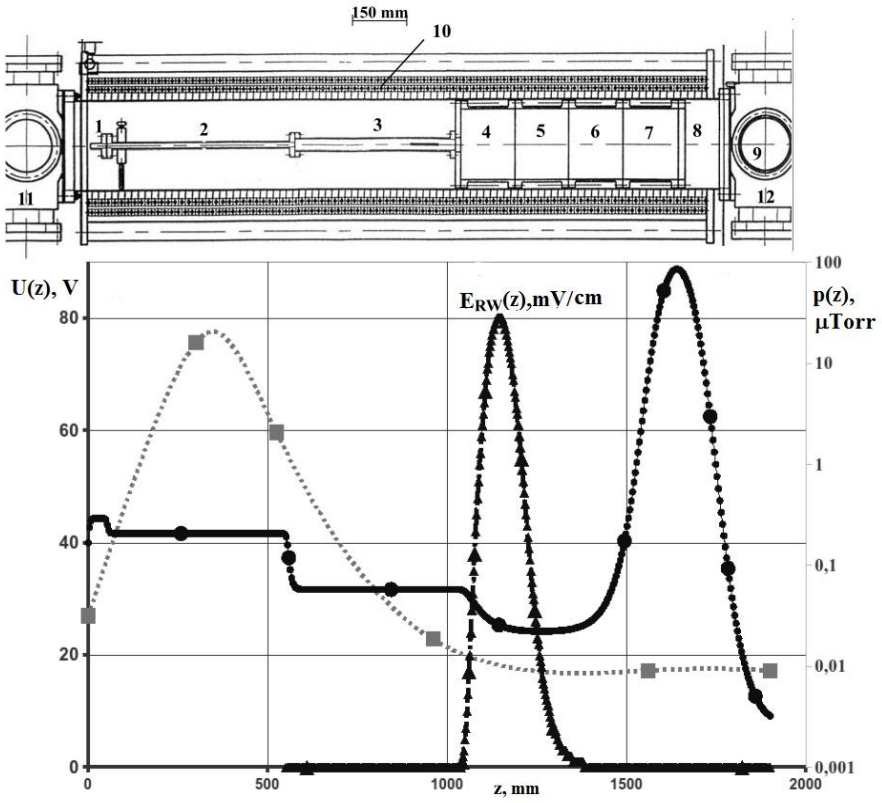

Fig. 17. A scheme of the PMS trap. 1-8 — electrodes, 4 — split (pie) electrode, with use to create the RW-field 9 — collector and scintillation counter, 10 — solenoid, 11 and 12 - turbomolecular and cryogenic vacuum pumps. Below — distribution of the potential U(z) of the electric field of the electrodes (●, numerical simulation) and the RW-field is ERW(z) (▲ , numerical simulation) and buffer gas pressure p(z) (■, measurement and calculation) on the axis of the trap in positron accumulation mode.

For measuring the transverse dimensions of the positron bunches was used a movable collector (Fig. 16, POS. 9) and scintillation counter.

In experiments on the electron, beam is formed by three-electrode gun with impregnated oxide cathode with a diameter of 2 mm. The potential of the cathode is 50 V. Selecting the duration and frequency of voltage pulses on the control electrode allows to specify the average flow of electrons, simulating the positron accumulation from a radioactive source.

The electrons accumulated in the trap, also thrown to the collector, and their charge is measured by current amplifier having an equivalent input resistance R = 300 ohms, a pulse duration (FWHM) of 1 μs. Accordingly, $N_{trap} = 2.1 \cdot 10^7 \cdot V_{[V]}$.

The transverse dimensions of the electron bunches was measured by luminescence of the phosphor in region 9 using the CCD camera.

The experiments were conducted to study the accumulation of electrons and positrons at different modes of the trap [2.17, 2.18, 2.19]. The process of accumulation is well described by the dependence of the accumulated particles number N_{bunch} from accumulation time at fixed values of the efficiency of capture ε, the fixed flow injected positron $\dot{N}$ and the lifetime of the particle in the trap τ.

$$N_{\text{bunch}}(t) = \varepsilon \dot{N} \tau (1 - e^{-t/\tau}) \Rightarrow \begin{cases} \varepsilon \dot{N} t, t << \tau, \\ \varepsilon \dot{N} \tau, t >> \tau \end{cases} \quad (1.6)$$

With a known flow $\dot{N}$ the first of the asymptotics allows us to determine the effectiveness value ε, and the second a value of ετ. In addition, the fitting of the experimental curve of the accumulation formula (1.6) gives an independent value of τ. Typical parameters for positrons: ε≈2-6 %, $\dot{N} \approx 10^4 c^{-1}, \tau \approx 10 - 20$c.

Fundamentally new results were obtained in studies of "RW-spectra" in experiments 2014-2015 [2.20, 2.21] (after the significant improvement of the vacuum conditions in the trap). When measurements of the number of particles in the bunch N_{bunch}, the efficiency of capture of particles in the accumulation ε and life-time τ in the trap from the frequency of the RW field was investigated in different modes — low and high — intensity of injected particle flows and accumulated bunches. Previously not observed low-frequency resonance of the RW field have been found, causing a significant increase in the number of accumulated particles. In addition, for the first time the effect of the "antiresonance" at low, on the order of tens of Hertz, the frequencies of RW-field, in which the rotation of the field leads to the complete destruction of the accumulated bunches (Fig. 18).

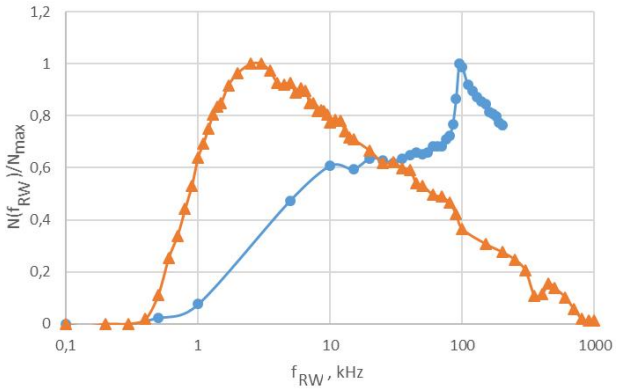

Fig. 18. The number of accumulated positrons ▲ and electrons ● (normalization to the maximum) vs the frequency of the RW field, kHz: amplitude of the RW field 1 V, pressure of the buffer gas in the accumulation of 2.75·μTorr.

The effectiveness of the RW field depends significantly on the potential distribution of the electrodes of the trap. The value of the resonance frequency grows exponentially with the number of particles in the bunch N_{bunch} (Fig. 19), and the efficiency of accumulation at the resonant frequency increases with particles accumulation $N_{bunch}(t)$, reaching a maximum and then decreases [2.20].

In 2014-2015, has been studied the dependence of the positron accumulation efficiency from the buffer gas pressure (table. 5). From the table it is seen that with increasing pressure the lifetime of the particles τ slowly falls, and the capture efficiency ε growing. The composition ετ is also growing. The activation of the RW field on the resonant frequency increases the number of accumulated particles more than double.

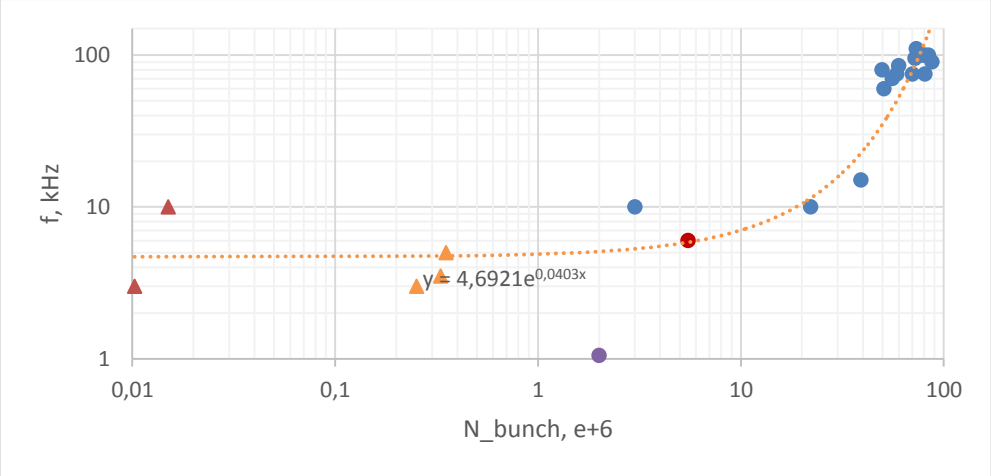

Fig. 19. The resonance frequency vs the number of particles N_{bunch}, accumulated over 20 s: ● electrons, ▲ — positrons; dotted line — the trend of y(x) = 4,6921 × exp(0,0403x)

Table 5. The dependence of parameters of accumulation of the pressure of the buffer gas

P, 10^{-6} Torr	τ, sec RW off/RW on	ε, % RW off/RW on	ε × τ, % × sec RW off/RW on	N_{bunch}, 10^5
1,1	4,5/12,5	1,5/1,4	6,75/17,5	0,3/0,7
4,0	5,0/8,5	6,5/7,1	32,5/60,3	1,2/2,2
7,0	5,0/9,0	11,5/11,3	57,5/101,7	1,7/2,9
10,1	5,0/7,5	16,3/17,2	81,5/129,0	2,0/3,3
13,7	3,5/6,0	25,6/23	89,6/138,0	2,1/3,2

The experimental results served as the basis for formulating a model of the mechanism of accumulation of the particles trapped in the PMS. The first part of the movement were formulated in [2.18]. Then after a series of experiments [2.20, 2.21] was built 3D-model that describes the particle accumulation in the trap. First, it became clear that the motion of particles trapped in the PMS can be divided into rapid longitudinal, along the axis of symmetry of the trap, and relatively slow, in a plane transverse to the axis (which was marked in our publication [17]). The characteristics of the longitudinal motion in the form of damped oscillations ("bounce-oscillations") are determined by the longitudinal component of the electric field of the electrodes and "friction" that occurs in collisions with buffer gas molecules. On lateral movements, the main effect of a homogeneous longitudinal magnetic field and radial component of the electric fields of the electrodes of the trap and the space charge of the accumulated bunch and the friction in the collision. Diffusion of particles in collisions with the buffer gas compensate the action of RW-field having the resonant nature of the accumulated particles.

In 2015, the mechanism explaining the effect of compression of positron bunches in a trap with longitudinal magnetic and rotating electric fields, has been fully formulated and confirmed experimentally [2.20]. It include the following.

The trajectory of the particle in the transverse plane in the region outside of the RW field is a result of the addition of the fast cyclotron rotation and slow "magnetron" rotation about the axis of symmetry of the static electric field traps and bunch. The friction occurring in

collisions, lead to compress of the orbits of the cyclotron rotation and unwinding of the trajectories in magnetron motion — diffusion of accumulated particles on the walls of the vacuum chamber, and death. A buffer gas necessary to capture particles in the area of accumulation, however, its action is greatly reduces the lifetime of the particles. The RW-field in electrode 4 (Fig. 18), being conservative, is able (as it may seem paradoxical!) reduce the size of the bunch, increase the life time of the particles and, as a consequence, increase the efficiency of their accumulation. This effect takes place (as already noted in [2.20]), if the frequency of the RW field is consistent with the frequency ω_{magn} of magnetron rotation and longitudinal oscillations of the particles. Otherwise, the time average effect of the RW field is zero. In the area of RW-field the particle from the initial entry point (x_0, y_0) in the field moves in a circular path of radius

$$R_{RW}(z) = cE_{RW}(z)/B\omega_{RW} \tag{1.7}$$

with centre in point

$$(x_0 - R_{RW} \cdot \cos\alpha, y_0 - R_{RW} \cdot \sin\alpha), \tag{1.8}$$

where E_{RW} and ω_{RW} — amplitude and frequency of the RW field B = 0.1 T constant magnetic field of the trap solenoid, α is the angle between the vector E_{RW} and the x-axis at the time of entry (Fig. 20). This is the result of exact solutions of the equations of particle motion under constant field along the z axis, E_{RW} field and "magnetized" particles (larmor radius is much less than R_{RW}).

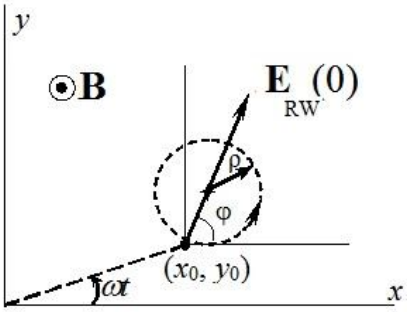

Fig. 20. Trajectory of "magnetized" particles in the area of RW-field; the trap axis at x = y = 0

Over time τ_{RW} stay in the RW-field particle passes a segment of the arc $\Delta s = R_{RW}\omega_{RW}\tau_{RW}$ of circle, offset to the trap axis, if at the time of entry of the angle α is the optimal value. A special case of such trajectories is shown in Fig. 21.

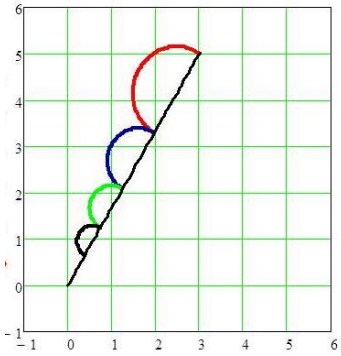

Fig. 21. The particle trajectory in the area of RW-field with multiple "bounce"-oscillations; the axis of the trap at x = y = 0, α = 59°, $(R_{RW})^n = k^{n-1}(R_{RW})_1$, k = 0.7, n = 1, 2,..., $(R_{RW})_1$ = 1.0; frequency ω_{RW} selected that the particle in the area of RW-field makes a half turn.

For the period of longitudinal oscillations of the particles T_{bounce}, RW-field vector rotated by the same angle $\Delta\phi_{RW} = \omega_{RW} \cdot T_{bounce}$ and the particle is displaced in azimuth relative to the trap axis on the angel

$$\Delta\phi_e = \int_0^{T_{\text{bounce}}} \omega_{\text{magn}}(t)\text{dt} + \omega_{\text{RW}}\tau_{\text{RW}}\, \Delta\varphi_e = \int_o^{\tau_{bounce}} \omega_{magn}(t) \cdot dt_{magn} + \int_o^{\tau_{RW}} \omega_{RW}(t) \cdot dt \text{ ,(1.9)}$$

where τ_{RW} — the particle staying time in the RW-field. From the equality $\Delta\varphi_{RW} = \Delta\varphi_e + 2\pi n$, n is an integer, followed by the resonance condition:

$$\Delta\varphi_e = \int_0^{T_{bounce}} \omega_{magn}(t)dt + \omega_{RW}\tau_{RW} \tag{1.10}$$

This formula is "3D-resonance" — approximation. It's just when

$$\Delta s << R_{RW}, \text{ или } \omega_{RW}\tau_{RW} << 1. \tag{1.11}$$

Thus, the main characteristics and conditions 3D resonance can be formulated in the following way:

1. The angular velocity of “magnetized” particle rotation in a circular orbit in RW-field does not depend on the particle energy.

2. The radius of the “magnetized” particle trajectory (circle) in the RW-field proportional to the field strength E_{RW}.

3. The period of longitudinal oscillations depends weakly on the particle energy (quasiparabolic the potential of the field electrodes of the trap $U(z)$).

4. Particles rotate around trap axis under the action of crossed fields longitudinal magnetic and radial components of the electric field of the trap electrodes and the space charge of the bunch of accumulated particles when move in trap.

5. 3D resonance occurs when the conditions (1.10), (1.11).

The obtained results provide an explanation of the longstanding problem of explaining the resonance action of the RW field on the process of accumulation of particles. The results obtained by the authors, allow to choose the parameters of the PMS trap, allowing it to form bunch of charged particles of high intensity and hold them for a long time with the purpose of their use in fundamental and applied research (e.g., positron annihilation spectroscopy of materials). Development and improvement of methods of accumulation of particles allows to advance in the formulation of experimental studies of a new generation. This series of works has allowed to obtain results at the level of modern science in this area.

There are some limitations on the maximum number of particles stored in the trap N. The limit of the space charge is determined by the departure of the particle from the electric potential well. For a cylindrical bunch of length L and radius R_b, the potential of the space charge on the axis of the bunch is described by the formula [32]

$$\phi_0 = e\frac{N}{L}\left(1 + 2\ln\frac{R}{R_b}\right), \tag{1.12}$$

where R is the radius of the electrodes in the accumulation area. Upon reaching such values of N, when

$$\phi_0 \geq \Delta\phi_{3-4}, \tag{1.13}$$

($\Delta\phi_{3-4}$ - the potential between electrodes 3 and 4) potential well "opens up" and ceases to hold the particles.

Another limitation of the particle density in the trap n_B imposes a " Brillouin criterio " [33] is the condition under which pushing forces of space charge and centrifugal forces of the rotating bunch superior the magnetic component of the Lorentz force of the magnetic holding field:

$$n_B \le \frac{B^2}{8\pi mc^2}. \qquad (1.14)$$

For positrons in the magnetic field of 0.1 T, this criterion gives $n_B = 5\cdot10^{10}$ cm^{-3}. For light particles — electrons and positrons — the limit is set primarily by the space charge. Limit the electron number in a bunch can be estimated from the conditions (1.12), (1.13):

$$N_{\max} = \frac{\Delta U \cdot L}{e \cdot \left(1 + 2\ln\frac{R}{R_b}\right)}. \qquad (1.15)$$

For $R_b \approx 0.5$ cm, $R = 10$ cm, $L = 30$ cm and $\Delta U = 10$ V this estimate gives $N_{max} = 3\cdot10^8$, which agrees well with the experimental result $N_{exper} = 1{,}3\cdot10^8$ (the maximum number of accumulated electrons in the trap).

In the accumulation mode have been measured leak currents to the electrodes. It turned out that the electrons do go to the electrode 3. Leak currents on the other electrodes below the noise level of 0.5 pA. These results are a direct confirmation of the mechanism of limiting the number of accumulated particles by the effect of space charge is described above (formula (1.15)).

A second confirmation of this hypothesis is an experiment to study the effect of dynamic increase of the depth of the potential well in the accumulation process: the accumulation of electrons, the depth of the potential well force increased, which allowed to accumulate $N^*_{exper} = 2\cdot10^8$. This value is 1.3 times larger than the maximum number of accumulated particles without the use of dynamic methods of increasing the depth of the potential well[*)].

3. Positron Annihilation Spectroscopy

3.1 Three PAS methods

Positron annihilation spectroscopy (PAS) is a sensitive method for the detection of various (so-called "open-volume") defects with a size from 0.1 to 1 nm with a minimum concentration of 10^{-7} cm^{-3} (the ratio of the defect number to the number of atoms per unit volume of the substance). PAS method has better space resolution than transmission electron microscope (transmission electron microscope — TEM) by 4 orders. There are many publications reporting successful use of the PAS method in studies of the plastic deformation [3.1, 3.2], shear deformation [3.3], slice [3.4], etc.

Create a monochromatic positron beam of variable energy will find wide application in the PAS method, for example, in the study of radiation defects [35, 36] or thin films [37, 38]. This was confirmed by the first PAS experiments [39]. Slowing and monochromatization of a positron flux from a radioactive source opens the opportunity to trace changes in the structure

[*)] After this experiment we have discovered the publication [24], which describes a similar method. The authors were able to increase the number of accumulated particles in 1.5 times

of the material in thin layers, starting from the sample surface, which is impossible in the traditional PAS method on the positron flux with a wide range of energies.

Cryogenic positron source CSSMP allows to create a flux of low energy positrons that meets the requirements of the PAS methods. An additional possibility of adjusting the energy of the positrons appears when the sample is "hung" under negative potential, which accelerates the positrons that allows implementing monoenergetic positrons of a specified energy into the sample that penetrate to a certain depth.

In contrast to heavy particles (ions) electrons in a substance are not moving on the straight (mostly) trajectory, but diffuses, undergoing scattering at large angles. Therefore, for electrons the semiempirical formula for the average depth of penetration is introduced:

$$h = (A/\rho) \cdot E^{n}_{[\text{keV}]}. \qquad (3.1)$$

Here h is the average depth, ρ is the density in g/cm^3, A, n — constants determined by numerical simulations. So, for the iron calculation based on the program GEANT4 gives A = $2{,}62 \cdot 10^{-6}$ g/(cm^2·keV), n = 1,1692 [3.10].

There are three experimental PAS methods.

The first observation of the angular correlation of the annihilation gamma quanta. This method is used in fundamental research, which include the distribution of pulses of electrons and the Fermi surface. Its application is hindered by the bulkiness of the necessary equipment and lack of its production industry. In this regard, the method is rarely used.

The second method is the measurement of the lifetime of positrons in matter ("Positron Annihilation Lifetime Spectroscopy" - PALS). It allows determining the type, size and concentration of defects by increasing the positron lifetime that is proportional to the volume of the defect. This method can be used as the standard experiments on special isotopes such as ^{22}Na and pulsed beams of positrons with a specific temporal reference.

The third method is based on the Doppler effect — the change in energy of the annihilation gamma-quanta ("Doppler Broadening of the Annihilation Line" – DBAL). This method is used for detection of vacancies, vacancy clusters and their concentrations. The annihilation of captured by defect positron gives a narrower spectrum of annihilation line 511 keV in comparison with that which is created in the annihilation of the positron with the electrons of the atoms of an ideal structure or conduction electrons.

This difference is caused by the formation of defect — free cavities the above-mentioned "nano-scale", in which a positron freely lives, elastically bouncing off the walls of the cavity until annihilate with an electron of one of the wall atoms. In an ideal structure, the positron is scattered by the structure atoms as elastic and inelastic. Inelastic scattering increases the spread of the positrons at the energy and, accordingly, the amount of Doppler broadening of annihilation gamma-quanta.

Shape analysis of the obtained gamma spectra is a standard for PAS by calculating the so-called S-parameter (Fig. 27). It is equal to the ratio of the area under the curve of the gamma spectrum in the "reference" interval to the area of the gamma spectrum in the full (infinite) interval of the energy of the detected photons. Reference (reference) interval $\Delta\varepsilon_{ref}$ of energies is determined by gamma spectrum of the reference ("ideal") sample from the conditions.

$$S_{ref} = \frac{A_S}{A} \sim 0{,}5\,.$$

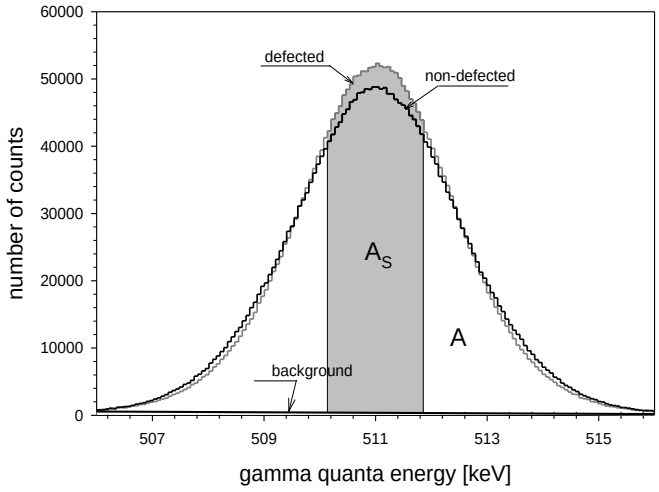

Fig. 22. Gamma spectra lines of reference (non-defected, black line) and deformed (defected, gray line) samples; $\Delta\varepsilon_{ref} \approx 1{,}65$ keV.

Then measurements of S-parameter for spectra of the studied ("defective") samples makes. The difference of the areas under the curves of gamma-ray spectra in the range $\Delta\varepsilon_{ref}$ for the reference and the deformed (strain slip) samples clearly seen in Fig. 22.

The procedure of measuring the distribution of defect concentration is as follows. The dependence of S parameter on the energy of the positron $S(E_p)$ is taken (therefore, from the depth h). The experimental results for the reference and "defective" samples is fitted by using the VEPFIT program [3.11, 3.12]. The values of two "adjustable" parameters — S_{sat} —S-parameter value corresponding to the saturation curve S(Ep) at Ep → ∞ (Fig. 27) are determined, and the L_{pdl} — positron path length in matter (the positron diffusion length). To determine the concentration of defects, use the following formula

$$C_{\text{def}} = \frac{1}{\tau_{\text{ref}}\mu} \cdot [(\frac{L_{\text{ref}}}{L_{\text{pdl}}})^2 - 1], \tag{3.2}$$

where τ_{ref} is the positron lifetime in a reference sample obtained from independent experiments of PAS according to the method of measurement of the lifetime, μ is the parameter obtained by the numerical simulation [40], C_{def} is the maximum concentration of defects, which is achieved when the saturation factor $S(E_p) = S_{sat}$.

3.2. DBAL spectrometer

Doppler PAS Method is currently used on the injector of positrons. The spectrometer DBAL is made by a standard scheme (Fig. 28). It consists of a high voltage source, HpGe detector, a preamplifier, a multichannel analyzer and computer. For registration of gamma quanta produced in positron annihilation is used HpGe detector of Baltic Scientific Instruments. The detector has the following parameters: the relative efficiency of detection of 1.33 MeV γ-quanta (according to IEC 60973) is equal to 30 %; energy resolution (FWHM at 511 keV) is less than 1.25 keV. the energy range of the detector lies in the range from 40 keV to 10 MeV. The detector is powered by a voltage source of 6 kV, made in the NIM standard by the same company.

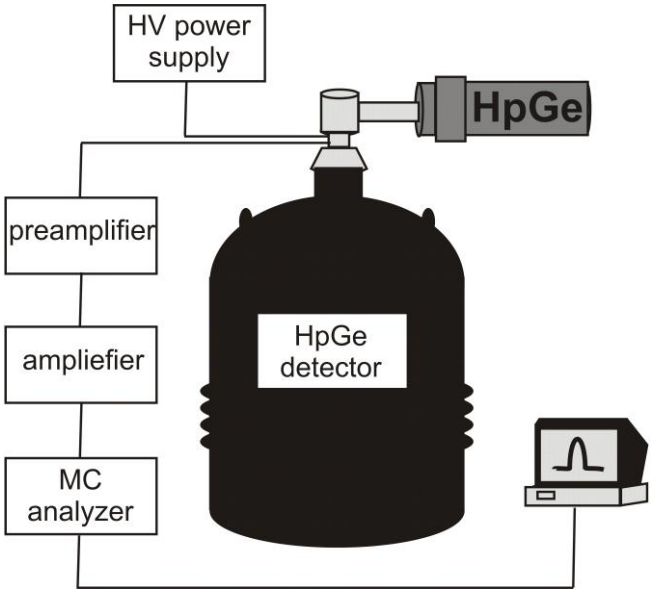

Fig. 23. Scheme of DBAL spectrometer.

The investigated samples are placed in a vacuum chamber at the exit of the trap (Fig. 16, POS. 5) on the axis of the direct flux of positrons from CSSMP (the potentials of the electrodes of the trap in this case equal to zero). Samples are placed on a movable vacuum input to which is supplied an adjustable negative potential up to 35 kV. The annihilation gamma-quanta are registered by the HpGe detector, which has a resolution of 1.2 keV at a quanta energy 511 keV. The detector is placed in a recess ("pocket") of the vacuum chamber as close as possible to the irradiated sample.

The signal after passing through the detector (preamplifier integrated in the detector) is amplified in the amplifier ORTEC 572 A and fed to multichannel analyzer TUKAN 8k with 8192 channel resolution associated with the computer. Thus, the spectra of the annihilation process obtained and S-and W - parameters calculated. The approximate measurement time of about one hour.

In the example shown in Fig. 24, shows the curves $S(E_{positron})$ for samples of iron, the implanted ions Xe^{26+} with an energy of 167 MeV at the cyclotron IC-100 FLNR of JINR.

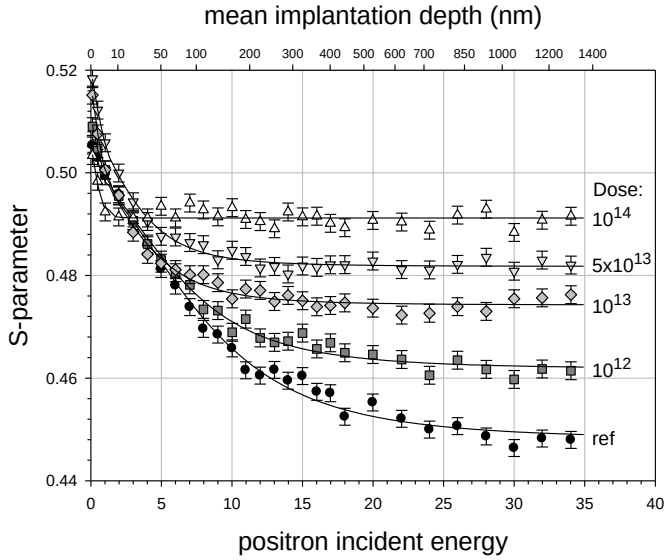

Fig. 24. S-parameter vs the positron energy for the reference ("ref") and "defected" samples implanted ions Xe^{26+} with an energy of 167 MeV and curves fitting (description in the text); the picture shows the irradiation dose, ion/cm^2

The results of studies of various materials by DBAL PAS in 2012-2015, published in [3.14–3.19]. Further development of the method PAS in 2016-2018 is discussed in section 4.

4. The development of experiment technique

In 2015 had started the preparation work, that allows reaching the intensity of the accumulated particles 10^7 in the injector, and also extending the experimental potential of the complex for PAS. With this aim was bought in iThemba LABS fresh positron emitter based on the ^{22}Na isotope an activity of 30 μCI and cryocooler by Sumitomo company. A new version of the source have been developed, that allow its cooling from cryocooler in a closed cycle, which significantly increased the efficiency works on the positrons (section 4.1).

4.1. CSSMP

A significant problem when working on the positrons is use liquid helium for CSSMP cooling that transported in dewars. This significantly limits the time (shortage of liquid helium) and requires long, about 6-7 hours preliminary preparation of the source why the working day is stretched to 12-13 hours. In this regard, efforts have been made for the acquisition of Sumitomo company cryocooler and the development of new CSSMP design, designed to work with the cooling helium in a closed cycle. By September 2015. source CSSMP-2 was constructed and its elements are made (Fig. 25). Completion and beginning of the "cold" tests were conducted during 2016, and in November the source was installed to the injector of slow positrons and tested.

a) b) c)

Fig. 25. Source CSSMP-2: a) interior, b) the developers of the source V. Seleznev, and V. M. Drobin demonstrate the basic elements of front of full assembly, c) CSSMP installed on a regular place.

After the commissioning of the source, it gave the opportunity to accumulate in the trap bunch intensity of 3×10^6 positrons.

4.2. Creation of PALS spectrometer

Spectroscopy by the PALS method can be performed on the positrons, from an independent source of ^{22}Na. This isotope through 3.3 ps after the positron emission emits gamma quantum with energy of 1274 keV, which is used as a trigger signal of the spectrometer for the measurement of the lifetime (Fig. 26). The stop signal is the registration of gamma quantum with the energy 511 Kev. The time difference of both signals and gives the value of the positron lifetime. The positron source is covered by two thin foils (about 5 microns) and placed between two identical samples. This "sandwich" is placed in front of two counters (scintillators and photomultipliers Fig. 26) BaF_2. The PALS spectrometer is used PEM Hamamatsu. To analyze signals in the coincidence is used lifetime spectrometer APV8702 and computer. Usually, for the analysis of time are required number of modules of measurement of radiation, such as differential CFD, delay lines, TAC, MCA, etc In AP 8702 they are all integrated. The result is a spectra of the positron lifetime, and subsequent analysis allows to estimate the lifetime of the positron in the sample.

After creation of a slow monochromatic positron specialized channel (SMPSC, section 4.3) with the ordered positrons (section 4.4) this instrument will be moved to the experimental station (Fig. 27A, POS.4), what allow to study samples by the PALS method at a controlled depth.

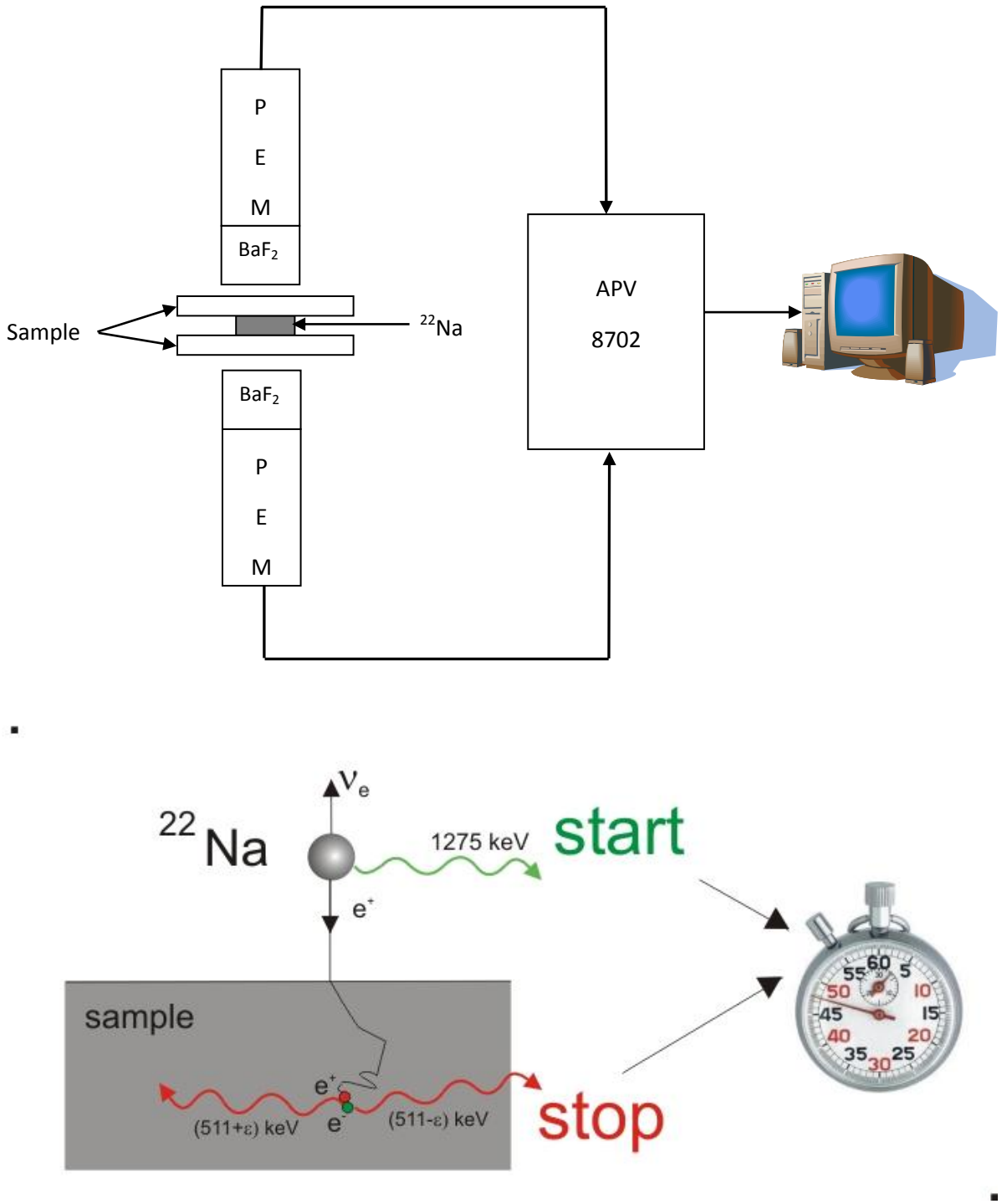

Fig. 26. Scheme of positron lifetime measurement in PALS method

4.3. Slow monochromatic positron specialized channel

Designed (Fig. 27), manufactured and mounted the slow monochromatic positron specialized channel (SMPSC). Started developing devices to form an orderly flow of positrons. This will allow to create PAS, based on the measurement of the positron lifetime in matter.

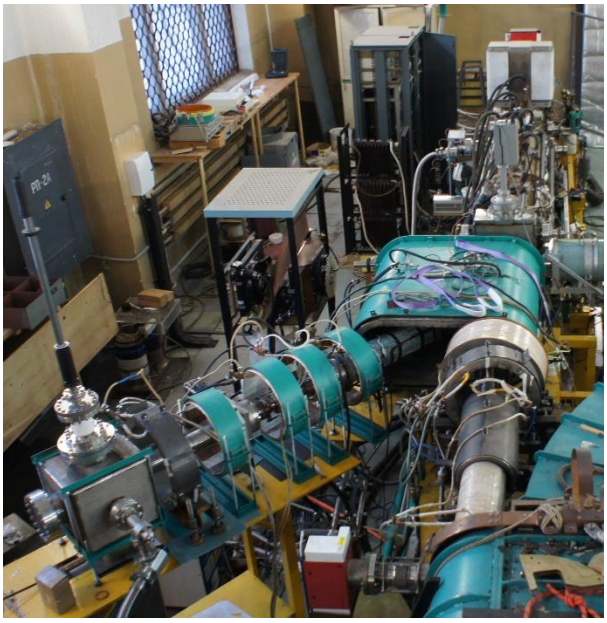

Fig. 27. Slow monochromatic positron specialized channel (SMPSC) 1 - positron transport channel into the ring, 2 – positron transport channel to the station PASS.

SMPSC can work in two modes — direct-flying and deflected beams. Accordingly, the channel is equipped with two sets of coils that generate a magnetic field: the coil creates a longitudinal field transport direct-flying beam (Fig. 27, pos. 1), and coils transport the rejected beam (Fig. 27, pos. 2).

4.4. The ordering flux of positrons

PAS method application based on the measurement of the lifetime of positrons in matter is possible on the relatively rare single positron flux. The interval between the moments of contact positrons with the target should be several times larger than the characteristic life time of a positron in matter τ_{life} ~ 100 PS. Accordingly, the maximum flux of positrons on the target

$$\frac{dN}{dt} \leq \frac{1}{10\tau_{life}} \sim 10^9 c^{-1},$$

that is certainly satisfied for most modern PAS installations based on a radioactive source of positrons. Thus as the trigger used for the measurement of the time interval between the arrival of the positron on target and its annihilation in the material, the use of gamma-quanta, accompanying β^+-decay of the nuclei in the emitter of positrons. It is clear that in this formulation of the experiment, positron monochromaticity is excluded — is too large and uncertain time of positron diffusion in slowing down matter source. Hence, the uncertainty of the energy of the positrons.

In our project is proposed to form an ordered flux of monochromatic positrons. To do this, a beam of monochromatic positrons passes U_{RF} section (Fig. 28), where a high frequency (RF) voltage of a special form is applied. Further, the positrons are accelerated in a static electric field on high voltage gap U_A and come to target U_{target}.

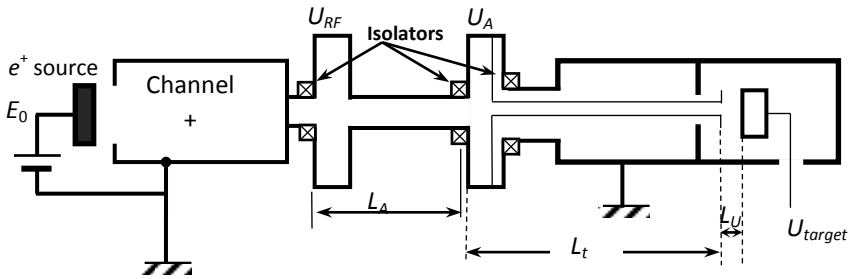

Fig. 28. Scheme of positron flux ordering (explanation in text).

The form of the RF signal, we find as follows.

Consider that the positron enters RF cavity (U_{RF}) at time t_{inj} (injection) with periodicity in average every $T_0 = \left(\dot{N}_{e+}\right)^{-1}$~2 μs and energy $E_0 + \delta E, \delta E \sim \pm 1$ eV. The positron speed at the exit of an RF cavity is equal to

$$v_{RF}(\delta E, t_{inj}) = \sqrt{\frac{2}{m} \cdot (E_0 + \delta E + eU_{RF}(t_{inj}))}, 0 \le t_{inj} \le T_0. \quad (4.1)$$

The flight time from the RF cavity to the section U_A is $\Delta t_A = \frac{L_A}{v_{RF}}$.

Positron velocity after passing accelerating part is

$$\frac{mv_A^2}{2} = \frac{mv_{RF}^2}{2} + eU_A$$

$$v_A(\delta E, t_{inj}) = \sqrt{v_{RF}^2 + \frac{2}{m} eU_A}. \quad (4.2)$$

With this velocity the positron is flying the section of the channel of the length L_t and comes to the entrance of the chamber where the sample to be studied is placed under a negative potential U_{target}. Time of positron flight from the entrance of the RF cavity to the entrance of the accelerating gap of the chamber is equal to

$$t_{target} = t_{inj} + \Delta t_A + \frac{L_t}{v_A(E, t_{inj})} = t_{inj} + \frac{L_A}{v_{RF}} + \frac{L_t}{v_A}. \quad (4.3)$$

We find the function $U_{RF}(t)$ from the condition of equality of values Δt_{target} for positrons having energy E_0 (i.e. $\delta E = 0$) at any t_{inj} value

$$0 \le t_{inj} \le T_0, \quad (4.4)$$

or

$$\Delta t_{target}(t_j = 0) = \Delta t_{target}(t_{inj} \le T_0). \quad (4.5)$$

In this case, all particles, regardless of t_{inj}, arrive at the target simultaneously. Then we have:

$$\frac{L_A}{v_{RF}(0,0)} + \frac{L_t}{v_A(0,0)} + t_{inj} + \frac{L_A}{v_{RF}(0, t_{inj})} + \frac{L_t}{v_A(0, t_{inj})}. \quad (4.6)$$

This equation for the function $U_{RF}(t_{inj})$ is solved by the method of successive approximations.

1st approximation:

$$\frac{L_A}{U_{RF}} \gg \frac{L_t}{U_A}. \quad (4.7)$$

From (4.6) we find

$$\frac{L_A}{v_{RF}^{(1)}(0,0)} = t_{inj} + \frac{L_A}{v_{RF}^{(1)}(0,t_{inj})}. \quad (4.8)$$

Taking $U_{RF}(0) = 0$, from (4.8) we obtain (when δE = 0!)

$$U_{RF}^{(1)}(t_{inj}) = [\frac{1}{(1-\sqrt{\frac{2E_0}{m}}\frac{t_{inj}}{L_A})^2} - 1] \cdot E_0, \quad (4.9)$$

$$v_A^{(1)}(0, t_{inj}) = \sqrt{\frac{2}{m} \cdot (E_0 + eU_{RF}^{(1)}(t_{inj}) + eU_A)}. \quad (4.10)$$

2nd approximation:

We present the equation (4.6) as following:

$$\frac{L_A}{v_{RF}^{(2)}(0,0)} = t_{inj} + \frac{L_A}{v_{RF}^{(2)}(0,t_{inj})} + \delta t_2, \quad (4.11)$$

where

$$\delta t_2 = L_t(\frac{1}{v_A^{(1)}(0,t_{inj})} - \frac{1}{v_A^{(1)}(0,0)}), \quad (4.12)$$

Hence

$$U_{RF}^{(2)}(t_{inj}) = [\frac{1}{(1-\sqrt{\frac{2E_0}{m}}\frac{t_{inj}+\delta t_2}{L_A})^2} - 1] \cdot \frac{E_0}{e}. \quad (4.13)$$

$$v_{RF}^{(2)} = \sqrt{\frac{2}{m} \cdot (E_0 + \delta E + eU_{RF}^{(2)})},$$

$$v_A^{(2)} = \sqrt{\frac{2}{m} \cdot (E_0 + \delta E + eU_{RF}^{(2)}(t_{inj}) + eU_A)}.$$

The positron flight time at initial energy E_0+δE is equal to

$$t_{target}(\delta E, t_{inj}) = t_{inj} + \frac{L_t}{v_A^{(2)}(\delta E, t_{inj})} + \frac{L_A}{v_{RF}^{(2)}(\delta E, t_{inj})}. \quad (4.14)$$

We are interested of the difference between the time of positron arrival at the target for positrons with δE ≠ 0 and δE = 0

$$\delta t_{target}(\delta E, t_{inj}) = t_{target}(\delta E, t_{inj}) - t_{target}(0, t_{inj}). \quad (4.15)$$

We consider two version of the U_{RF} formation: using a digital generator and a set of three or four generators of harmonic voltage which have frequency harmonics of the frequency $\frac{2\pi}{T_0}$ that allow us to form $U_{RF}^{(2)}(t)$ voltage. As the preliminary analysis has shown three harmonic signals (i.e., the three generators) are sufficient.

In Fig. 29 – 31 we present the results of calculations by formulas (4.1) – (4.15) for the version of U_{RF} formation with a digital generator for the chosen values of parameters of a positron flux and the channel: E_0 = 100, 120, 200 eV, δE_0 = ±1 eV, T_0 = 10 ns, L_A = 15 cm, L_t = 2.5 m, U_A = 5000:

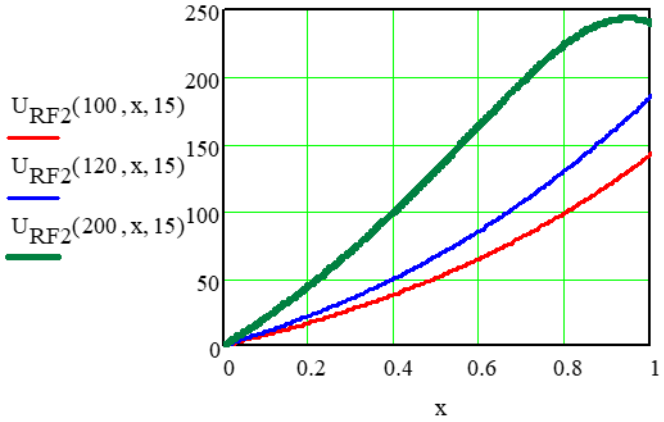

Fig. 29. The pulsed voltage (volts) vs time $t=xT_0$ of the positron entry of the into the U_{RF} section at the energy E_0 = 100, 120, 200 V.

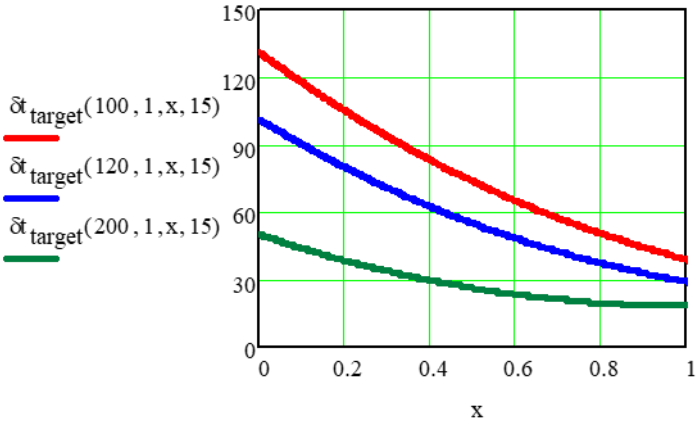

Fig. 30.The difference between the arrival time of positrons at the target (ps) depending of time $t=xT_0$ of the positron entry into the U_{RF} section with the energy E_0 = 100, 120, 200 V, $\delta E0$ = 1эВ.

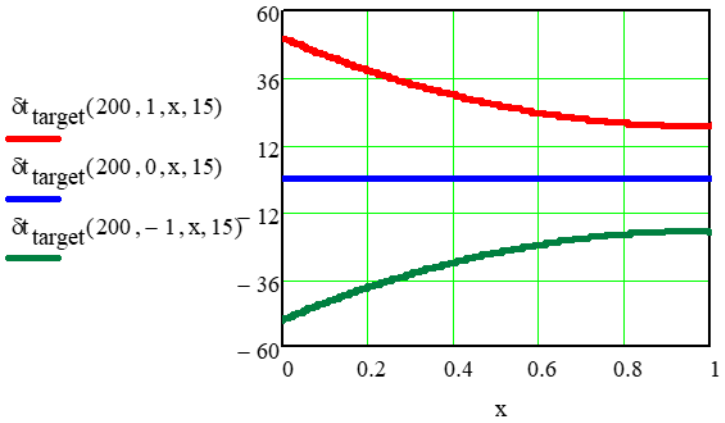

Fig. 31.The difference between the arrival time of positrons at the target (ps) from time $t=xT_0$ of the positron entry into the U_{RF} part with the values E_0 = 200 V, $\delta E0$ = 0, ±1эВ.

5. Expected outcomes upon completion of the project

1. The development of the positron annihilation spectroscopy (PAS) method and research materials by this method:

1.1. Construction and commissioning of the positron transport channel and experimental station.

1.2. Creation PAS method based on the measurement of the positron lifetime in matter.

2. Optimization of the positron accumulation in the trap — the achievement of intensity of 10^7 positrons per cycle.

5.1. The results expected in 2018

1. The commissioning of the slow monochromatic positron specialized channel (SMPSC) and the experimental station. Beginning of the researches by the DBAL method.

2. Research by PALS method at the low activity source ("table-top" experiment").

3. Creation a test version of the device forming an orderly flux of positrons.

4. Optimization of the positron accumulation in the trap.

5.2. The results expected in 2019.

1. The creation of devices forming an orderly flux of positrons in SMPSC.

2. Research by the DBAL and PALS methods at the low activity source.

3. Research by DBAL method at the ordered flux of slow monochromatic positrons.

5.3. Expected results in 2020

1. The creation of the PALS spectrometer on SMPSC.

2. Research by the DBAL and PALS methods at the low activity source.

3. Research by DBAL and PALS methods on the flux of slow monochromatic positrons.

Conclusion

The implementation of the program presented in this project will bring the complex to a qualitatively new level, will create new opportunities for experimental researches with ordered positron flux.

Literature

I. 1. I. N. Meshkov, A. N. Skrinsky, The antihydrogen and positronium generation and studiesnusing storage rings. NIM A, 391, 1997, p. 205

I. 2. И. Н. Мешков, Экспериментальные исследования физики антиводарода и позитрония. Проблемы и возможности. Experimental studies of antihydrogen and positronium physics: Problem and Possibilities. ЭЧАЯ, т. 28 (2), 1997, сс. 495-540. Phys. Part. Nucl., 28(2), 1997, pp. 198-215.

I. 3. А. О. Сидорин, А. В. Смирнов, Г. В. Трубников, И. А. Селезнёв, Е. М. Сыресин. Модифицированный бетатрон. ЭЧАЯ, т. 36 (5), 2005, сс. 1071-113.

1.1 V. Slugen, H. Hein, S. Sojak, J. Veternikova, Irradiation induced damage of the reactor pressure vessel steels studied by positron annihilation lifetime techniques.

1.2 S. van der Zwaag, A. Van Veen, H. Schut, A. J. Hill and T. J. Bastow, Determination of Fatique Damage at Precipitate Level in 2024-T3 using Positron Annihilation and Nuclear Magnetic Resonance, Procidings of the 9th International Conference on Aluminium Alloys,

2004, p. 363 – 368
1.3 Jana Simeg Veternikova, Jarmila Degemova, Vladimir Slugen, Applicability of Positron Annihilation Method for Corrosion Study, 2014
1.4 J. Cizek, I. Prochazka, R. Kuzel, Z. Matej, V. Cherkaska, M. Chelar, B. Smola, I. Stulikova, G. Brauer, W. Anwand, R. K. Islamgaliev and O. Kulyasova, Ulta Fine-Grained Metals Prepared by Severe Plastic Deformation: A Positron Annihilation Study, Acta Physica Polonaca A, vol. 107 (2005), No. 5, p. 745 – 752
1.5 Lijuan Zhang, Tao Wang, Ji Li, Yingping Hao, Jindang Liu, Peng Zhang, Bin Cheng, Zhongwei Zhang, Baoyi Wang, Bangjiao Ye, Thin Solid Films, 525 (2012), p. 68-72
1.6 Z. Q. Chen, S. Yamamoto, M. Maekawa, A. Kawasuso, X. L. Yuan and T. Sekiguchi, Postgrowth annealing of defects in ZnO studied by positron annihilation, x-ray diffraction, Rutherford backscattering, cathodoluminescence, and Hall measurements, Journal of Applied Physics, vol. 94, number 8, 2003, p. 4807 – 4812
1.7 Junqing Yan, Guangjun Wu, Naijia Guan, Landong Li, Zhuoxin Li and Xingzhong Cao, Phys. Chem. Chem. Phys, 2013, 15, p. 10978 – 10988
1.8 M. F. Ferreira Marques, C. Lopes Gil, P. M. Gordo, Zs. Kajcsos, A. P. de Lima, D. P. Queiroz, M. N. de Pinho, Radiation Physics and Chemistry, 68, 2003, p. 573 – 576
1.9 Alexandra L. Howie, Positron Annihilation Lifetime Spectroscopy of Metals, Semiconductors, Thin Films and Zeolites, Thesis for Bachelor of Science, Centre for Antimatter-Matter Studies at School of Physics, UWA
2.1. R. H. Howell, I. J. Rosenberg and M. J. Fluss, Applied Physics A 43, (1987), p. 247–255.
2.2. C.A. Kapetanakos, A Technique for generating potent positron beams, Journal of Synchrotron Radiation 3, (1996), p. 268–271.
2.3. F.Ebel et al, Hyperfine Interactions, 44, (1989), p. 179–183.
2.4. T. Nakano et al., Experiment at SPring-8, Nucl. Phys. A 670, (2000), p. 332.
2.5. M.Fedurin, G.Kulipanov, N.Mezentsev and V.Shkaruba, Superconducting high-field three-pole wigglers at Budker INP, Nucl. Instr. and Meth. in Phys. Res. A 448, (2000), p. 51.
2.6. L.Madansky and F. Rasetti, Phys. Rev. 79 (1950), p. 397.
2.7. W.H. Cherry, Secondary electron emission produced from surfaces by positron bombardment, Ph.D. Dissertation, Princeton University, (1958).
2.8. D.G. Costello, D.E. Groce, D.F. Herring, G. Wm. MacGovan, Phys. Rev. B 5, (1972), p.1433.
2.9. Jr. Mills, L. Pfeifer, Phys. Rev. Lett. 43, (1979), p. 1961.
2.10. A. P. Mills, Jr. and E. M. Gullikson, Solid Neon Moderator for Producing Slow Positrons, Appl. Phys. Lett. 49, (1986) p. 1121.
2.11. В.Ф.Быковский, А.Г.Кобец, Е.В.Болтушкин, В.Н.Малахов, И.Н.Мешков, В.Н.Павлов, Р.В.Пивин, И.А.Селезнев, В.Г.Шмаровоз, С.Л.Яковенко, Инжектор позитронов для накопителя LEPTA, письма в ЭЧАЯ 3, (2006), p. 63–67.
2.12. L. V. Jørgensen, D. P. van der Werf, T. L. Watson, M. Charlton and M. J. T. Collier, in Nonneutral Plasma Physics IV, edited by F. Anderegg, L. Schweikhard and C. F. Driscoll (American Institute of Physics, New York, 2002), Vol. AIP 606, (2002), p. 35
2.13. D. P. van der Werf, L. V. Jørgensen, T. L. Watson, M. Charlton, M. J. T. Collier, M. Doser and R. Funakoshi, Appl. Surf. Sci. 194, (2002), p. 312.
2.14. F.J.Wysoci, M.Leventhal, et al., Hiperfine Interaction 44, (1988), p.185–200.

2.15. X. P. Huang, et al., Phys. Rev. Lett. 78, (1997) 875.
2.16. Ахманова Е.В., Есеев М.К., Кобец А.Г., Мешков И.Н., Рудаков А.Ю., Сидорин А.А., Яковенко С.Л. Проект LEPTA: формирование и инжекция позитронного пучка// Письма в ЭЧАЯ 9, (2012) 618–623.
2.17. Akhmanova, E.V., Eseev, M.K., Kobets, A.G., Meshkov, I.N., Rudakov, A.Y., Sidorin, A.A., Yakovenko, S.L. LEPTA project: Formation and injection of positron beam, PEPAN Letters 9 (4–5), (2012) 373–376.
2.18. Eseev M.K., Ahmanova E.V., Vititnev A.N., Kobets A.G., Meshkov I.N., Rudakov A.Yu. , Sidorin A.A., Yakovenko S.L., Compression and Confinement of Positron Clouds in the Surko Trap of Lepta Facility, Proc. of RUPAC2012, St.Peterburg, Russia, 2012, (CERN: JACoW) 319–321.
2.19. Есеев М.К., Кобец А.Г., Мешков И.Н., Рудаков А.Ю., Яковенко С.Л. Исследование накопления заряженной плазмы в ловушке с вращающимся электрическим полем установки LEPTA, Физика плазмы, 39, 883–890 (2013).
2.20. Eseev M.K., Kobets A.G., Meshkov I.N., Rudakov A.Yu., Yakovenko S.L. Study of Nonneutral Plasma Storage in a Magnetic Trap with a Rotating Electric Field at the LEPTA Facility, Plasma Phys. Rep., 39 (10), 787–794 (2013).
2.21. E. Ahmanova, M. Eseev, A. Kobets, V. Lokhmatov, I. Meshkov, O. Orlov, V. Pavlov, A. Rudakov, A.A. Sidorin, S. Yakovenko. LEPTA project: towards positronium // Proc. of COOL2013, Murren, Switzerland, 2013, (CERN: JACoW) 119–120.
2.22. Есеев М.К., Кобец А.Г., Мешков И.Н., Сидорин А.А., Орлов О.С. Механизм накопления заряженных частиц в ловушке Пеннинга-Малмберга-Сурко с вращающимся электрическим полем, Письма в ЖЭТФ, 102 (5), 291–296 (2015).
2.23. Eseev M.K., Kobets A.G., Meshkov I.N., Sidorin A.A., Orlov O.S. The Mechanism of Accumulation of Charged Particles in a Penning–Malmberg–Surko trap with a Rotating Electric Field, JETP Letters, 102 (5), 261–265 (2015)].
2.24. Eseev M.K**.**, Ahmanova E., Kobets A., Meshkov I., Orlov O., Sidorin A., Yakovenko S., Mechanism of Compression of Positron Clouds in the Surko Trap of Lepta Facility, Proc. of RUPAC-2014, Obninsk, Russia, 2014, (CERN: JACoW) 20–22.
2.25. C.F. Driscoll, in Low Energy Antimatter, edited by D.B. Cline (World Scientific, Singapore, 1986), p. 184–195.
2.26. L. Brillouin, Phys. Rev. 67, (1945), p.260.
2.27. C.M. Surko, C.M. Gilbert and R.G. Greaves, Progress in Creating Low-Energy Positron Plasma and Beams, in Non-Neutral Plasma Physics III, edited by J.J. Bollinger, R.G. Spencer and R.C. Davidson, AIP Conference Proceedings 498, New York, 1999, p. 3–12.
2.28. И.Н. Мешков, А.Н. Скринский, Nucl. Instr. And Meth., 1996, v. A379, p. 41.
3.1. I.N.Meshkov, A.O.Sidorin, A.V.Smirnov, E.M.Syresin, G.V.Trubnikov, Particle Dynamics in the sectional modified betatron, NIM A 441 (2000), Nos 1–2, p. 267.
3.2. I.Meshkov, Y.Korotaev, A.Sidorin, A.Smirnov, E.M.Syresin, I.Titkova, High perveance electron gun for the electron cooling system, NIM A 441 (2000), Nos 1–2, p. 92.
3.3. Мешков И.Н., Сидорин А.О., Смирнов А.В., Трубников Г.В., Electron Cooling of Positrons in LEPTA, Hiperfine Interaction, 2003, v. 146/147, (1/4), 197–201.
3.4. E. Dryzek , M. Sarnek, M. Wróbel, Reverse transformation of deformation-induced martensite in austenitic stainless steel studied by positron annihilation, J. Mater. Sci. 49

(2014) 8499–8458.
3.5. E. Dryzek, M. Sarnek, K. Siemek, Annealing behaviour of plastically deformed stainless steel 1.4307 studied by positron annihilation methods, Nukleonika 58 (2013) 215−219.
3.6. J. Dryzek, M. Wróbel, Positron studies of subsurface zone in titanium created in sliding wear, Tribol. Lett. 55 (2014) 413–419.
3.7. P. Horodek, J. Dryzek, M. Wróbel, Positron annihilation study of defects induced by various cutting methods in stainless steel grade 304, Tribol. Lett. 45 (2012) 341–347.
3.8. J. Simeg Veternikova, V. Slugen, S. Sojak, M. Skarba, E. Korhonen, S. Stancek, J. Degmova, V. Sabelova, I. Bartosova, Application of slow positron beam for study of commercial oxide-dispersion-strengthened steels, J. Nucl. Mater. 450 (2014) 99–103.
3.9. J. Jiang, Y.C. Wu, X.B. Liu, R.S. Wang, Y. Nagai, K. Inoue, Y. Shimizu, T. Toyama, Microstructural evolution of RPV steels under proton and ion irradiation studied by positron annihilation spectroscopy, J. Nucl. Mater. 458 (2015) 326–334.
3.10. S.T. Kao, S.H. Huang, D.J. Liaw, W.C. Chao, C.C. Hu, C.L. Li, D.M. Wang, K.R. Lee, J.Y. Lai, Interfacially polymerized thin-film composite polyamide membrane: positron annihilation spectroscopic study, characterization and pervaporation performance, Polym. J. 42 (2010) 242–248.
3.11. P. Horodek, K. Siemek, A.G. Kobets, M. Kulik, I.N. Meshkov, Positron beam and RBS studies of thermally grown oxide films on stainless steel grade 304, Appl. Surf. Sci. 333 (2015) 96–103.
3.12. J. Dryzek, P. Horodek, GEANT4 simulation of slow positron beam implantation profiles, Nucl. Instrum. Methods Phys. Res. B 266 (2008) 4000–4009.
3.13. A. Van Veen, H. Schut, M. Clement, A., Kruseman, M.R., Ijpma, J.M.M. De Nijs VEPFIT applied to depth profiling problems, Appl. Surf. Sci. 85 (1995) 216–224.
3.14. J. Dryzek, The solution of the time dependent positron diffusion equation valid for pulsed beam experiments. Nucl. Instrum. Method. Phys. Res. B 196 (2002) 186–193.
3.15. A. Vehanen, P. Hautojärvi, J. Johansson, J. Yli-Kauppila, P., Moser, Vacancies and carbon impurities in α-iron: Electron irradiation. Phys. Rev. B 25 (1982) 762–780.
3.16. J. Dryzek, P. Horodek, K. Siemek, The slowing down times of positrons emitted from selected β^+ isotopes into metals, Nucl. Instrum. Meth. B 291 (2012) 22–28.
3.17. P. Horodek, J. Dryzek, A.G. Kobets, M. Kulik, V.I. Lokhmatov, I.N. Meshkov, O.S. Orlov, V. Pavlov, A.Yu. Rudakov, A.A. Sidorin, K. Siemek, Slow Positron Beam Studies of the Stainless Steel Surface Exposed to Sandblasting, Acta Phys. Polon. 125 (2014) 714–717.
3.18. P. Horodek, M. Bugdol, A.G. Kobets, I.N. Meshkov, O.S. Orlov, A.Yu. Rudakov, A.A.Sidorin, S.L. Yakovenko, Development of positron annihilation spectroscopy at LEPTA facility, Phys. Part.and Nucl.Lett. 11 (5) (2014) 708–712.
3.19. J. Dryzek, P. Horodek, The solution of the positron diffusion trapping model tested for profiling of defects induced by proton implanted in stainless steel, Appl. Phys. 121 (2015) 289–295.

Appendix 1. A list of purchased equipment

1. Vacuum equipment:

Production station HiCube 80	6 thousand$
Schieber (2 PCs)	12 thousand$
The bushings	5 thousand$

2. Diagnostic instrument bundles:

Ortec germanium detector	40 thousand$
Digital signal processor APU8002RU	14 thousand$
Software APU8002RU for APU8002RU	6 thousand$
The photomultiplier Hamamatsu	4 thousand$
The scintillator	500 $
Converter time-amplitude Ortec 567	6 thousand$

3. High-voltage equipment

HV power supply 100 kV	10 thousand$

4. RF equipment

RF generator + power amplifier	12 thousand$

5. Materials 15 thousand$